

# A fundamental plane of black hole activity

Andrea Merloni, Sebastian Heinz & Tiziana Di Matteo

*Max-Planck-Institut für Astrophysik, Karl-Schwarzschild-Strasse 1, D-85741, Garching, Germany*

## ABSTRACT

We examine the disc–jet connection in stellar mass and supermassive black holes by investigating the properties of their compact emission in the X-ray and radio bands. We compile a sample of  $\sim 100$  active galactic nuclei with measured masses, 5 GHz core emission, and 2–10 keV luminosities, together with 8 galactic black holes with a total of  $\sim 50$  simultaneous observations in the radio and X-ray bands. Using this sample, we study the correlations between the radio ( $L_R$ ) and the X-ray ( $L_X$ ) luminosity and the black hole mass ( $M$ ). We find that the radio luminosity is correlated with *both*  $M$  and  $L_X$ , at a highly significant level. In particular, we show that the sources define a “fundamental plane” in the three-dimensional ( $\log L_R, \log L_X, \log M$ ) space, given by  $\log L_R = (0.60^{+0.11}_{-0.11}) \log L_X + (0.78^{+0.11}_{-0.09}) \log M + 7.33^{+4.05}_{-4.07}$ , with a substantial scatter of  $\sigma_R = 0.88$ . These results support the notion that the properties of the inner jets from black holes are invariant under changes in black hole mass and accretion rate, as recently suggested by Heinz & Sunyaev (2003). We compare our results to the theoretical relations between radio flux, black hole mass, and accretion rate derived by these authors. Such relations depend only on the assumed accretion model and on the observed radio spectral index. Therefore, we are able to show that the X-ray emission from black holes accreting at less than a few per cent of the Eddington rate is unlikely to be produced by radiatively efficient accretion, and is marginally consistent with optically thin synchrotron emission from the jet. On the other hand, models for radiatively inefficient accretion flows seem to agree well with the data.

**Key words:** accretion, accretion disks – black hole physics – X-rays: binaries – galaxies: active – radio continuum: general – X-rays: general

## 1 INTRODUCTION

The ultimate observational evidence of a celestial body being a black hole comes from dynamical studies, by measuring the gravitational influence of the central object on neighboring stars and gas, both in binary systems and in the nuclei of galaxies. However, there are a number of distinctive signatures of black hole-powered activity that are usually regarded as proxy of black hole existence. Relativistic jets emitting synchrotron radiation in the radio band are one such signature, the second most common being the presence of strong, compact power-law X-ray emission commonly associated with the inner part of an accretion flow. Indeed, as a general property, accretion onto compact objects and the launch of relativistic outflows/jets seem to be correlated (or *symbiotic*, Falcke & Biermann, 1995) phenomena (Begelman, Blandford, & Rees 1984; Rawlings & Saunders 1991). This implies that, at some level, a correlation between jet and disc flux is unavoidable.

Observationally, jet morphologies and spectral properties of both radio and X-ray cores are remarkably similar in the case of black holes of stellar mass (galactic black holes, hereafter GBH) and of their supermassive counterparts (hereafter SMBH) in the nuclei of galaxies. If jets are launched in the innermost parts of the accretion flows, as commonly assumed, then these similarities

suggest that it should be possible to understand the physics of both black hole accretion and jet production by studying all those systems as a *single* class. To this end, radiation emerging at radio and (hard) X-ray frequencies is the most direct probe of the immediate vicinity of the black hole: effects of extinction are unimportant in the radio band, while in the X-rays, as far as the absorber are not Compton thick, such an effect can be accounted for with good enough spectral capabilities. Thus, radio and X-ray observations, together with the information on the central black hole mass, should allow us to study the relationship between the fundamental parameters characterizing black hole activity such as the central black hole mass,  $M_{\text{BH}}$ , and the accretion rate,  $\dot{M}$ , as well as the disc–jet coupling.

Until less than ten years ago, quasars and active galactic nuclei, and the supermassive black holes believed to power them, were regarded as exceptional (and extreme) objects. However, beginning with the work of Kormendy & Richstone (1995) and, in particular, Magorrian et al. (1998), the idea that SMBH reside in the nuclei of virtually every galaxy in the nearby universe has become almost commonplace. In addition, the tight correlations found between black hole mass and bulge luminosity (and therefore mass; Magorrian et al. 1998), and between black hole mass and bulge ve-

lucity dispersion (Gebhardt et al. 2000; Ferrarese & Merritt 2000), are now regarded as fundamental tools to understand the growth and activity of SMBH. A complementary picture of the demographics of local SMBH comes from the work of Ho, Filippenko, & Sargent (1997b), who have carried out a detailed optical spectroscopic survey of a large number of nearby galaxies. From this work, it was found that between a third and a half of the sample has AGN-like spectra, albeit of low luminosity, (LLAGN; either of the LINER, Seyfert or Transition type; see Ho, Filippenko, & Sargent 1997a), thus confirming that SMBH are not only present in galaxies, but that they are also active (at least at some level). As a matter of fact, follow-up radio surveys of optically selected LLAGN (Ho & Ulvestad 2001; Nagar et al. 2002) have yielded extremely high detection rates, with the radio emission having predominantly a compact core morphology, occasionally accompanied by jet-like features. X-ray studies at arcsecond (or sub-arcsecond) resolution with the *Chandra* X-ray Observatory have also allowed us to firmly pin down the emission properties of the nearby dim galactic nuclei through systematic surveys of LLAGN (Ho et al. 2001; Terashima et al. 2002; Terashima & Wilson 2003). These pieces of information on local, low-luminosity objects nicely complement those on more luminous (and more distant) “classical” AGN (i.e. Seyfert galaxies, QSOs, radio galaxies) and should allow us to investigate the possible dependences of observable properties on black hole mass and perhaps accretion rate.

Alongside the work on black hole demographics, there have been various claims for the existence of a correlation between radio luminosity or radio loudness (a measure of the ratio of radio to bolometric luminosity) and SMBH masses (Franceschini, Vercellone, & Fabian 1998; McLure & Dunlop 2001; Lacy et al. 2001; Nagar et al. 2002; Laor 2000). Comparisons of radio emission from GBH and SMBH has also led to the suggestion that there is a systematic difference in radio loudness between the two classes, SMBH being on average more radio loud (Falcke & Biermann 1996; Fender & Kuulkers 2001). However, the difficulty of separating the dependence of the radio power output on the accretion rate (due to the lack, or the neglect, of an independent observational indicator of it) unavoidably makes the evidence of any such correlation rather weak. Indeed, other authors, using different samples, have recently found no evidence for such correlations (Ho 2002a; Woo & Urry 2002; Oshlack, Webster, & Whiting 2002).

A link between the disc accretion rate and the generation of relativistic radio jets has been suggested by Willott et al. (1999) for radio galaxies and by Ho & Peng (2001) for Seyfert 1 nuclei, on the basis of the strong observed correlations between radio and optical powers. Moreover, by studying a sample of galactic nuclei with measured black hole masses, Ho (2002) found clear evidence of radio loudness being anti-correlated with some estimator of the dimensionless accretion rate. Interestingly, Brinkmann et al. (2000) have also correlated the ROSAT All-Sky Survey and the VLA FIRST catalog, and have shown that there is some degree of correlation between the monochromatic X-ray luminosity at 2 keV and the radio (5 GHz) luminosity for bright AGN and Quasars (for both radio loud and radio quiet sources), while Sambruna et al. (1999) have found a weak correlation between lobe radio power and 2-10 keV luminosity in a sample of radio loud AGN.

The situation is rather different for GBH where the measured black hole masses span a very narrow range (around 10 solar masses). In this case, the observed, rather large, changes in luminosity can only be explained if they are somehow linked to variations in the accretion rate. On this note, re-

cent work has shown that GBHs in the low/hard state (where their spectra are dominated by a power-law X-ray emission with typical bolometric luminosities  $L_{\text{bol}}/L_{\text{Edd}} \lesssim 10^{-2}$ ) often possess compact radio cores the radio luminosity of which is tightly correlated with their X-ray luminosity over more than three orders of magnitude (Gallo, Fender, & Pooley 2002; Gallo, Fender, & Pooley 2003; Corbel et al. 2003). The evidence of such a correlation emphasizes the effects of the dependence of the radio luminosity on the accretion rate (and not only on the black hole mass) and hence the connection between accretion and jet processes. However, the tightness of the correlation has also led some authors (Markoff et al. 2003; Corbel et al. 2003) to the suggestion that the X-ray emission in low luminosity black hole systems is due to synchrotron radiation from the jet, thus challenging the standard view that it originates in the accretion flow itself.

Finally, we should also note that GBH with bolometric luminosity close to their Eddington limit display a more complicated behavior when observed in the radio band. There is evidence that in the high/soft state (when the spectral energy distribution is dominated by a quasi-thermal component with  $kT \sim 1$  keV) continuous jet production is inhibited, while at still higher luminosities (in the so-called very high state) powerful, episodic super-luminal ejection events have been observed (in particular in the prototypical micro-quasar GRS 1915+105, Mirabel & Rodriguez, 1994). Thus, high luminosity black hole X-ray binaries seem to display a (temporal) dichotomy between radio loud and radio quiet states, perhaps reminiscent of that of powerful quasars.

This rapid (albeit somewhat disorderly) progress in the observational studies of black holes of all classes seems to offer the possibility for understanding fundamental scalings of black hole properties with  $M_{\text{BH}}$  and  $\dot{M}$ . Accretion disc theory can provide us with the relationships between the observed radiative output (hence X-ray luminosity) and the black hole masses and accretion rates. Unfortunately, theoretical modeling of the relation between jet properties (related to the observed radio luminosity) and the physical parameters of the system ( $M_{\text{BH}}$ ,  $\dot{M}$ ) has been hampered by the lack of a clear understanding of the mechanism by which jets are accelerated and collimated. Relating the X-ray and radio properties of a black hole system to only  $M_{\text{BH}}$  and/or  $\dot{M}$  has not been straightforward. However, in a recent paper, Heinz & Sunyaev (2003) have demonstrated that, under the general assumption that the jet formation process is not qualitatively different among SMBH of different mass or between SMBH and GBH, it is in fact possible to derive a universal scaling between the jet (radio) luminosity at a given frequency,  $L_{\nu}$ , and both mass and accretion rate. The derived relation is *independent of the jet model* and has scaling indices that depend only on the (observable) spectral slope of the synchrotron emission in the radio band, and on the accretion model (see § 5 below).

Motivated by these findings, the aim of this work is twofold. First, we want to examine (or re-examine) the significance of the correlations between radio and X-ray luminosities with  $M_{\text{BH}}$  and with each other in a large sample of black holes with measured masses that includes *both* GBH and SMBH. Then, we will make use of the model by Heinz & Sunyaev (2003) to relate observed relations to theoretical predictions. This will allow us to make some progress in our understanding of accretion processes and of the disc-jet coupling in different regimes of black hole activity.

The structure of the paper is as follows: we describe the selection criteria and the properties of our sample in §2. In §3 and §4 we present the results of the correlation analysis and in §5 we present a physical interpretation of these results. Section 6 is devoted to a discussion of our findings and of their general implications for

our understanding of black hole activity. Finally we summarize our results in §7

## 2 THE SAMPLE

### 2.1 Supermassive black holes in galactic nuclei

We have selected from the existing literature a sample of black hole-powered systems with measured masses, the nuclei of which have been observed both at 5 GHz (mostly with arcsecond resolution with the VLA) and in the 2–10 keV band. For future reference we define the dimensionless black hole mass  $M = M_{\text{BH}}/M_{\odot}$  and accretion rate  $\dot{m} \equiv (L_{\text{bol}}/\eta)/L_{\text{Edd}} = \dot{M}c^2/L_{\text{Edd}} \propto \dot{M}/M$ , where  $\eta$  is the accretion efficiency.

We first considered the full sample of  $\sim 40$  nearby inactive, or weakly active galaxies with existing nuclear black hole mass measurements from observations of spatially resolved kinematics. To these we have added a comparable number of bright AGNs (and QSOs) with nuclear black hole mass measured from reverberation mapping of their broad line region (a similar sample was compiled by Ho et al. 2002). From this sample we selected all objects which have been observed in both the radio and X-ray bands.

In order to obtain a more statistically representative sample, we also searched the existing literature for both nearby low-luminosity galactic nuclei (Ho et al., 2001; Terashima et al., 2002; Nagar et al., 2002; Terashima & Wilson, 2003) and for relatively bright Seyfert nuclei (either type 1, type 2 or Narrow Line Seyfert 1) and radio galaxies with available radio and X-ray flux measurements. We assign black hole masses to these systems using the observed correlation between black hole masses and stellar velocity dispersion (Gebhardt et al. 2000; Ferrarese & Merritt 2000)<sup>1</sup>, mostly using the values of the velocity dispersion provided by the HYPERLEDA catalogue (Simien & Prugniel 2002).

We do not include in our sample BL Lac objects, for which beaming is important, or distant quasars, for which the  $M - \sigma$  relation cannot be used because of the lack velocity dispersion measurements. In practice, we want to avoid any indirect method for black hole mass estimation that relies on e.g. the continuum optical/UV luminosity (as done by Woo & Urry, 2002, for example).

We note here that it is beyond the scope of this paper to discuss the different methods (and their qualities) for estimating black hole masses in the nuclei of galaxies, and refer the reader to the comprehensive literature on the subject (see e.g. De Zeeuw, 2003, and references therein).

### 2.2 Galactic black hole sources

The Galactic X-ray binaries included in our sample have been selected to have (a) simultaneous X-ray and radio observations, or *RXTE* All-Sky-Monitor (ASM) X-ray data in conjunction with radio fluxes available from the literature, and (b) publicly available *RXTE*-ASM X-ray and Green-Bank Interferometer (GBI) radio lightcurves (from which we estimated the 5 GHz fluxes by interpolating between the 2.25 GHz and the 8.3 GHz channels).

We treated the GBI and ASM data of each object in the following way: we first re-gridded the ASM X-ray lightcurve to the

<sup>1</sup> We use here the relationship  $M = 1.3 \times 10^8 (\sigma/200 \text{ km s}^{-1})^{4.58}$ , as derived in Ferrarese (2002). See however Tremaine et al. (2002) for a thorough statistical discussion of the different scalings that have been claimed for the  $M - \sigma$  relation.

radio lightcurve, and then sorted the data into bins of ascending X-ray flux. This procedure assumes that individual bins are not correlated and can thus be re-ordered and rebinned to improve statistics. Rebinning the data in time intervals does not change the results significantly, but reduces the dynamic range in X-ray flux. In this sense, X-ray-flux-ordered binning produces a better representation of the scatter in this variable. Since the GBI becomes noise dominated below about 15 mJy, we conservatively chose to consider data at or below this value as upper limits and split the sample into detection and upper limits before binning. ASM fluxes were converted to 2–10 keV luminosities using the a conversion factor of  $3.2 \times 10^{-10} [\text{erg s}^{-1} \text{ cm}^{-2}]/[\text{cts s}^{-1}]$  (Grimm, Gilfanov, & Sunyaev 2002), which assumes a crab-like source spectrum.

Black hole masses for GBH are derived from stellar kinematics and we use the value provided in the literature. For the micro-quasar LS 5039, no mass estimate is available, and we assumed  $M_{\text{BH}} = 10 M_{\odot}$ .

### 2.3 Global properties of the sample

Our final sample (Table 1) comprises 149 entries, of which 99 are individual SMBH systems. The remaining 50 correspond to the observations of 8 different GBH at various luminosity levels. Out of these 8 sources, 5 are so-called X-ray transients (Cyg X-3, GRO J1655-40, GRS 1915+105, XTE J1118+480 and XTE J1859+226) and 3 persistent sources (Cyg X-1, GX 339-4 and LS 5039). The SMBH sample includes 14 Quasars; 19 Seyfert galaxies of type 1 (in this class we include all the Seyfert spectrally classified as types 1 to 1.9); 32 Seyfert 2 galaxies; 7 Narrow Line Seyfert 1 galaxies (NLS1); 11 Low-Ionization Nuclear Emission line Regions (LINERS) of type 1.9; 13 LINERS of type 2 and 2 LINER/HII Transition nuclei. Separating mass estimators into direct ones (stellar kinematics, maser emission, gas kinematics and, to a lesser extent, reverberation mapping) and indirect ones (all those that infer a measure of the central black hole mass from the observed  $M - \sigma$  relation), we can assess possible biases introduced in our sample by the different mass measurement techniques. 54 masses are measured indirectly (4 Sy1, 3 NLS1, 30 Sy2, 15 LINERS and the two transition objects) and 45 directly (all the 14 QSOs, 15 Sy1, 2 Sy2, 4 NLS1, 8 LINERS plus Sgr A\* and M 32).

For the radio and X-ray luminosities taken from the literature, we have assumed  $H_0 = 75 \text{ km s}^{-1} \text{ Mpc}^{-1}$ , correcting the quoted values when necessary. When available, we have included information on the radio spectral properties of the sources. In Table 1 we have marked all the sources with flat radio spectrum ( $\alpha_{\text{R}} < 0.4$ , where  $\alpha_{\text{R}}$  is the radio spectral index  $\alpha \equiv -\partial \ln L_{\nu}/\partial \ln \nu$  evaluated at the frequency  $\nu = 5 \text{ GHz}$ ) with flag (F). All the sources with  $\alpha_{\text{R}} > 0.4$  are instead classified as steep spectrum (S), while those for which the radio spectral index couldn't be determined are marked with a (U). Overall, we have 77 flat spectrum sources (32 SMBH and 45 GBH, respectively); 43 steep spectrum sources (38 and 5) and 29 for which the spectral slope is undetermined (all SMBH).

In Figure 1 we show the distributions of black hole masses, radio and X-ray luminosities and that of the ratio of their X-ray to the Eddington luminosity,  $L_{\text{X}}/L_{\text{Edd}} = L_{2-10 \text{ keV}}/1.3 \times 10^{38} M$ . It is worth emphasizing that the shape of those distributions reflects more the nature of our selection procedure rather than the global intrinsic properties of accreting black holes. For example, a precise measurement of the central black hole mass is a prerequisite for a given source to be included in the sample. As recently discussed by

**Table 1.** Radio and X-ray properties of black holes with measured masses

Object (1)	D(Mpc) (2)	SC (3)	Log $L_R$ (4)	$\alpha_R$ (5)	Ref (6)	Log $L_X$ (7)	Ref (8)	Log $M$ (9)	Method (10)	Ref (11)
Ark 564	99.0	NS1	38.59	U	1	43.74	2	6.5	$I_{[OIII]}$	3
Cyg A	224	S2/L2	41.43	F	11	44.22	59	9.4	G	58
Fairall 9	199.8	S1	<37.68	U	4	44.14	5,6	7.91	R	21
IC 1459	29.2	L2	39.71	F	4,53	40.66 <sup>†</sup>	9	9	S	10
IC 4269 (PKS 1333-33)	188	L1.9	39.68	S	11	41.20	12	9.1	$I_\sigma$	13
IC 4329A	65.5	S1	38.94	U	4	43.72	5	6.69	R	21
Mrk 3	52.0	S2	39.86	S	14,51	42.7	14,15	8.81	$I_\sigma$	16
Mrk 78	149	S2	39.86	S	14,53	<44	14	7.92	$I_\sigma$	16
Mrk 279	127	S1.5	38.78	S	4,49	43.72	5	7.62	R	21
Mrk 335	107	NS1	38.27	F	4,49	43.30	2,17	6.79	R	21
Mrk 348	60.0	S2	39.70	F	14,52	42.85	14	7.17	$I_\sigma$	16
Mrk 478	316	NS1	38.75	U	18	43.87	2	7.30	$I_{[OIII]}$	3
Mrk 507	216	NS1	38.78	U	1	42.97	2	7.10	$I_{[OIII]}$	3
Mrk 509	144	NS1	38.30 <sup>§</sup>	S	19,56	44.00	20	7.86	R	4
Mrk 573	69.2	S2	38.22	S	14,49	<43.00	14	7.25	$I_\sigma$	16
Mrk 590	109	S1.2	38.70	S	4,49	43.58	57	7.23	R	21
Mrk 766	51.7	NS1	38.32	S	1,22	42.90	2,6	6.64	R	21
Mrk 1066	48.4	S2	38.68	S	14,53	<41.85	14	6.93	$I_\sigma$	16
NGC 221 (M 32)	0.810	-	<33.3	U	67	35.97	67	6.40	S	68
NGC 315	66.2	L1.9	40.41	F	23	41.68	24	9.10	$I_\sigma$	16
NGC 1052	19.6	L1.9	39.86	S	25	41.57	24	8.29	$I_\sigma$	16
NGC 1068	14.4	S1.9	39.12	S	4,27	41.00	15	7.20	M	4
NGC 1275	70.1	S2	41.74	F	14,27	43.40	32,34	8.64	$I_\sigma$	16
NGC 1365	21.8	S1.8	38.80	S	53	40.60	24	7.66	$I_\sigma$	26
NGC 1386	11.6	S2	36.70	U	53	40.64	24	7.20	$I_\sigma$	16
NGC 1667	61.2	S2	37.34	S	14,27	40.05	15	7.93	$I_\sigma$	16
NGC 2110	31.2	S2	38.99	F	14,53	42.60	14,15	8.41	$I_\sigma$	16
NGC 2273	28.4	S2	37.83	S	27	41.40	15,24	7.27	$I_\sigma$	16
NGC 2787	7.5	L1.9	37.22	F	4,29	38.40	24,28	7.59	G	10
NGC 2841	12.0	L2	36.00	F	29	38.26	28	8.42	$I_\sigma$	30
NGC 2992	30.8	S2	38.64	U	14	42.10	14,15	7.75	$I_\sigma$	16
NGC 3031 (M81)	3.9	S1.5	36.82	F	4,29	39.90	24,28	7.79	S	4
NGC 3079	20.4	S2	38.39	F	27,50	40.20	15	7.65	$I_\sigma$	26
NGC 3147	40.9	S2	38.01	F	27,31	41.61	15,31	8.79	$I_\sigma$	26
NGC 3169	16.5	L2	37.19	F	31,54	41.35	31	7.91	$I_\sigma$	33
NGC 3226	15.4	L1.9	37.20	F	31,54	40.74	31	8.23	$I_\sigma$	34
NGC 3227	20.6	S1.5	37.94	S	4,27	41.99	5	7.59	R	21
NGC 3362	111	S2	38.47	S	14,49	<43.6	14	6.68	$I_\sigma$	16
NGC 3516	38.9	S1	37.98	S	4,27	43.20	5,6	7.36	R	4
NGC 3627	6.6	S2	35.45	F	29	<37.6	28	7.26	$I_\sigma$	30
NGC 3675	12.8	T2	<35.99	U	29	<37.99	28	7.11	$I_\sigma$	30
NGC 3998	14.1	L1.9	37.98	S	4,53	41.66	24	8.75	S	4
NGC 4051	17.0	NLS1	37.30	S	4,27	41.50	5,6	6.11	R	21
NGC 4117	124	S2	35.70	S	14	39.4 <sup>†</sup>	45	6.74	$I_\sigma$	16
NGC 4143	17.0	L1.9	37.16	F	29,31	40.03	31	8.32	$I_\sigma$	34
NGC 4151	20.3	S1.5	38.49	S	4,27	42.83	5,6	7.17	R	21
NGC 4203	14.1	L1.9	36.79	F	29,31	40.23	28,31	7.90	$I_\sigma$	30
NGC 4258	7.3	S1.9	35.94	F	4,29	40.52	35	7.60	M	4
NGC 4261 (3C 270)	29.6	L2	39.21	U	11	41.17	24	8.72	G	4
NGC 4278	9.7	L1.9	37.91	F	29,31	39.96	31	9.20	S	60
NGC 4321	16.8	T2	<36.17	U	29	<38.59	28	6.80	$I_\sigma$	30
NGC 4374 (M84)	18.4	L2	38.81	F	4,29	40.34	24	9.20	G	4
NGC 4388	16.8	S2	36.95	S	27	42.76	15	6.80	$I_\sigma$	26
NGC 4395	3.6	S1.5	35.56	S	4,27	39.50	36	<5.04	S	4
NGC 4450	16.8	L1.9	36.53	F	29	40.34	24	7.30	$I_\sigma$	26
NGC 4457	17.4	L2	<35.70	U	29	39.97	24	6.86	$I_\sigma$	26
NGC 4472	18.8	S2	36.69	S	27,29	<38.80	37	8.80	$I_\sigma$	38
NGC 4486 (M87)	16.1	L2	39.78	F	4,29	40.55	39	9.48	G	4
NGC 4494	9.7	L2	<35.65	U	29	38.86	28	7.65	$I_\sigma$	30

Table 1 – *continued*

NGC 4501	16.8	S2	36.20	S	27	40.28	14	7.90	$I_\sigma$	26
NGC 4548	16.8	L2	36.30	F	29	39.79	31	7.40	$I_\sigma$	26
NGC 4565	9.7	S1.9	36.15	F	29,31	39.56	31	7.70	$I_\sigma$	26
NGC 4579	16.8	S1.9	37.65	F	29,31	41.14	28,31	7.85	$I_\sigma$	26
NGC 4594 (M104)	9.8	L2	37.84	F	4,53	40.70	15	9.04	S	4
NGC 4636	17.0	L1.9	36.40	U	29	<38.43	37	7.90	$I_\sigma$	38
NGC 4725	12.4	S2	<35.90	U	29	39.16	28	7.49	$I_\sigma$	30
NGC 4736	4.3	L2	34.80	F	29	39.62	24	7.30	$I_\sigma$	26
NGC 5033	18.7	S1.5	36.79	S	27	41.00	24,28	7.30	$I_\sigma$	30
NGC 5194	7.7	S2	35.50	S	27	39.80	15	6.90	$I_\sigma$	16
NGC 5252	92.3	S2	38.96	S	14,49	42.97	14	8.12	$I_\sigma$	16
NGC 5273	21.3	S2	36.22	F	14,24	<42.0	14	6.37	$I_\sigma$	16
NGC 5347	31.2	S2	37.10	F	14,55	40.0 <sup>†</sup>	45	6.70	$I_\sigma$	16
NGC 5548	70.2	S1.5	38.58	S	4,27	43.55	5	8.03	R	21
NGC 5929	33.2	S2	38.30	S	14,49	40.7 <sup>†</sup>	45	7.22	$I_\sigma$	16
NGC 6166	116	S2	39.95	S	40	40.56	41	9.19	$I_\sigma$	26
NGC 6251	94.8	S2	40.93	S	4,53	42.15	15	8.73	G	4
NGC 6500	40.0	L2	38.90	F	31,54	40.11	31	8.28	$I_\sigma$	30
NGC 7469	66.6	S1	38.38	S	4,49	43.31	42	6.81	R	21
NGC 7672	53.2	S2	37.25	S	14,55	43.37	14	6.80	$I_\sigma$	16
NGC 7682	68.0	S2	38.88	S	14,49	<43.2	14	7.25	$I_\sigma$	16
NGC 7743	24.4	S2	36.99	S	27	39.71	24	6.47	$I_\sigma$	16
PG 0026+129	627	Q	40.17	U	4	44.44	43	7.73	R	21
PG 0052+251	690	Q	39.42	U	4	44.66	44	8.34	R	21
PG 0804+761	430	Q	39.41	U	4	44.26	43	8.28	R	21
PG 0844+349	268	Q	38.12	U	4	43.29	43	7.34	R	21
PG 0953+414	1118	Q	40.14	U	4	44.50	43	8.26	R	21
PG 1211+143	362	Q	41.08	U	4	43.61	43	7.61	R	21
PG 1226+023 (3C273)	705	Q	44.03	F	4,56	45.70	44	8.74	R	21
PG 1229+204	268	Q	38.45	U	4	44.29	44	7.88	R	21
PG 1307+085	690	Q	38.98	U	4	44.51	44	8.44	R	21
PG 1411+442	380	Q	38.71	U	4	43.53	43	7.90	R	21
PG 1426+015	366	Q	38.98	U	4	43.89	44	8.67	R	21
PG 1613+658	565	Q	39.75	F	4,56	44.34	44	8.38	R	21
PG 1700+518	1406	Q	40.92	S	4,53	<43.20	43	7.78	R	21
PG 2130+099	255	Q	38.89	S	4,56	43.55	44	8.16	R	21
3C120	138	S1	41.55	F	11,53	43.95	11	7.36	R	21
3C 390.3	241	S1	41.09	S	11	44.00	11	8.53	R	21
UGC 6100	116	S2	38.50	U	14	<43.6	14	7.72	$I_\sigma$	16
Sgr A*	0.008	-	32.50	F	62	33.34	63	6.41	S	64
Cyg X-1	0.0021	GBH	<29.44	F	61	36.44	61	1.06	S	69
Cyg X-1	0.0021	GBH	<29.45	F	61	36.57	61	1.06	S	69
Cyg X-1	0.0021	GBH	29.63	F	61	36.48	61	1.06	S	69
Cyg X-1	0.0021	GBH	29.65	F	61	36.57	61	1.06	S	69
Cyg X-1	0.0021	GBH	29.66	F	61	36.64	61	1.06	S	69
Cyg X-1	0.0021	GBH	29.24	F	72	36.58	61	1.06	S	69
Cyg X-1	0.0021	GBH	29.30	F	72	36.65	61	1.06	S	69
Cyg X-1	0.0021	GBH	29.18	F	72	36.66	61	1.06	S	69
Cyg X-3	0.009	GBH	<30.64	F	61	36.94	61	1.00	S	70
Cyg X-3	0.009	GBH	31.62	F	61	37.19	61	1.00	S	70
Cyg X-3	0.009	GBH	31.85	F	61	37.41	61	1.00	S	70
Cyg X-3	0.009	GBH	32.17	F	61	37.60	61	1.00	S	70
Cyg X-3	0.009	GBH	32.43	U	61	37.88	61	1.0	S	70
GRO J1655-40	0.0032	GBH	<29.76	F	61	36.64	61	0.85	S	65
GRO J1655-40	0.0032	GBH	<29.69	F	61	37.55	61	0.85	S	65
GRO J1655-40	0.0032	GBH	29.94	F	61	35.27	61	0.85	S	65
GRS 1915+105	0.0125	GBH	<30.89	F	61	38.17	61	1.20	S	65
GRS 1915+105	0.0125	GBH	<30.89	F	61	38.47	61	1.20	S	65
GRS 1915+105	0.0125	GBH	<30.89	F	61	38.73	61	1.20	S	66
GRS 1915+105	0.0125	GBH	31.60	F	61	38.25	61	1.20	S	66
GRS 1915+105	0.0125	GBH	31.76	F	61	38.40	61	1.20	S	66
GRS 1915+105	0.0125	GBH	31.76	F	61	38.65	61	1.20	S	66

**Table 1 – continued**

GX 339-4	0.004	GBH	29.91	F	7	36.48	7	1.00	S	8
GX 339-4	0.004	GBH	29.87	F	7	36.42	7	1.00	S	8
GX 339-4	0.004	GBH	29.89	F	7	36.40	7	1.00	S	8
GX 339-4	0.004	GBH	29.62	F	7	36.12	7	1.00	S	8
GX 339-4	0.004	GBH	29.71	F	7	36.12	7	1.00	S	8
GX 339-4	0.004	GBH	29.66	F	7	36.14	7	1.00	S	8
GX 339-4	0.004	GBH	29.45	F	7	35.81	7	1.00	S	8
GX 339-4	0.004	GBH	29.11	F	7	35.32	7	1.00	S	8
GX 339-4	0.004	GBH	28.34	F	7	34.21	7	1.00	S	8
GX 339-4	0.004	GBH	28.02	F	7	33.91	7	1.00	S	8
GX 339-4	0.004	GBH	28.38	F	7	33.84	7	1.00	S	8
GX 339-4	0.004	GBH	28.49	F	7	34.01	7	1.00	S	8
GX 339-4	0.004	GBH	<27.51	F	7	<33.34	7	1.00	S	8
GX 339-4	0.004	GBH	<27.25	F	7	33.19	7	1.00	S	8
LS 5039	0.003	GBH	29.80	S	61	35.62	61	1.00	-	-
LS 5039	0.003	GBH	30.09	S	61	35.45	61	1.00	-	-
LS 5039	0.003	GBH	30.07	S	61	35.67	61	1.00	-	-
LS 5039	0.003	GBH	30.09	S	61	35.81	61	1.00	-	-
LS 5039	0.003	GBH	30.08	S	61	35.96	61	1.00	-	-
XTE J1118+480	0.0018	GBH	<28.98	F	46	35.43	47	1.00	S	48
XTE J1118+480	0.0018	GBH	28.92	F	71	35.46	61	1.00	S	48
XTE J1118+480	0.0018	GBH	28.92	F	71	35.57	61	1.00	S	48
XTE J1118+480	0.0018	GBH	28.92	F	71	35.56	61	1.00	S	48
XTE J1118+480	0.0018	GBH	28.92	F	71	35.47	61	1.00	S	48
XTE J1118+480	0.0018	GBH	28.92	F	71	35.45	61	1.00	S	48
XTE J1859+226	0.011	GBH	<29.24	F	61	36.58	61	>0.88	S	71
XTE J1859+226	0.011	GBH	<29.30	F	61	36.65	61	>0.88	S	71
XTE J1859+226	0.011	GBH	29.18	F	61	36.66	61	>0.88	S	71

NOTE: Comments:  $\dagger L_X$  calculated from the known luminosity in the 0.3-8 keV band and the observed spectral index;  $\ddagger L_X$  calculated from the GIS count rate, assuming  $\Gamma = 2$  and  $\text{Log}(N_{\text{H}}) = 22.5$ ;  $\S L_{5\text{GHz}}$  extrapolated from observations at 8 GHz. Col.(1): Name of the object. Col. (2): Distance in Megaparsecs (for  $H_0 = 75 \text{ km s}^{-1} \text{ Mpc}^{-1}$ ). Col. (3): Spectral Class; GBH: Galactic black hole; L: LINER; S: Seyfert; NLS1: Narrow Line Seyfert 1; T: Transition object (LINER/H II); Q: Quasar. Col. (4) Logarithm of nuclear luminosity at 5GHz. Col. (5): Radio spectral index  $\alpha_R$  (where  $F_{\nu} = \nu^{-\alpha_R}$ ); F: flat spectrum ( $\alpha_R < 0.4$ ); S: steep spectrum ( $\alpha_R > 0.4$ ); U: undetermined. Col. (7) Logarithm of the intrinsic rest-frame luminosity in the 2-10 keV band. Col. (9) Logarithm of the black hole mass. Col. (10) Mass measurement method; S: stellar kinematics; G: gas kinematics; M: maser kinematics; R: reverberation mapping;  $I_{[\text{OIII}]}$ : inferred from the mass-[OIII] line-width correlation;  $I_{\sigma}$ : inferred from the mass-velocity dispersion correlation.

REFERENCES: (1) Ulvestad, Antonucci & Goodrich (1995); (2) Leighly (1999); (3) Wang & Lu (2001); (4) Ho (2002); (5) Weaver, Gelbord & Yaqoob (2001); (6) Nandra et al. (1997); (7) Corbel et al. (2003); (8) Hynes et al. (2003); (9) Fabbiano et al. (2003); (10) Tremaine et al. (2002); (11) Sambruna, Eracleous & Mushotzky (1999); (12) Pellegrini et al. (2003); (13) Saglia et al. (1993); (14) Polletta et al. (1996); (15) Bassani et al. (1999); (16) Woo & Urry (2002); (17) Gondoin et al. (2002); (18) Zhou & Wang (2002); (19) Thean et al. (2001); (20) Pounds et al. (2001); (21) Kaspi et al. (2000); (22) Ho & Peng (2001); (23) Gregory & Condon (1991); (24) Terashima et al. (2002); (25) Griffith et al. (1995); (26) Simien & Prugniel (2002) and HYPERLEDA Catalogue: <http://www-obs.univ-lyon1.fr/hypercat/>; (27) Ho & Ulvestad (2001); (28) Ho et al. (2001); (29) Nagar et al. (2002); (30) Barth, Ho & Sargent (2002); (31) Terashima & Wilson (2003); (32) Allen et al. (2001); (33) Hereudeau & Simien (1998); (34) Churazov et al. (2003); (35) Fabbiano et al. (1992); (36) Shih et al. (2003); (37) Loewenstein et al. (2001); (38) Merritt & Ferrarese (2001); (39) Di Matteo et al. (2003); (40) Giovannini et al. (1998); (41) Di Matteo et al. (2001); (42) De Rosa, Fabian & Piro (2002); (43) George et al. (2000); (44) Lawson & Turner (1997); (45) Moran et al. (2001); (46) Dhawan et al. (2000); (47) Frontera et al. (2001); (48) Wagner et al. (2001); (49) Rush, Malkan & Edelson (1996); (50) Becker, White & Edwards (1991); (51) Kojoan et al. (1980); (52) White, Giommi & Angelini (2000); (53) Véron-Cetty & Véron (2001); (54) Falcke et al. (2001); (55) Ulvestad & Wilson (1989); (56) Falcke, Malkan & Biermann (1995); (57) Turner & Pounds (1989); (58) Tadhunter et al. (2003); (59) Young et al. (2002); (60) Magorrian et al. (1998); (61) This work; (62) Melia & Falcke (2001); (63) Baganoff et al. (2001); (64) Schödel et al. (2002); (65) Orosz & Bailyn (1997); (66) Greiner, Cuby & McCaughrean (2001); (67) Ho, Terashima & Ulvestad (2003); (68) Verolme et al. (2002); (69) Dolan (1992); (70) Hanson, Still & Fender (2000); (71) Filippenko & Chornock (2001); (72) Stirling et al. (2001); (73) Fender et al. (2001); .

De Zeeuw (2003), not all mass ranges are equally well probed by the different methods, and this should introduce a strong selection effect in our sample. Similarly, because BH masses are more easily measured in the nuclei of nearby galaxies, our sample is biased against the most luminous quasars. This should be taken into account when examining, for example, the  $L_X/L_{\text{Edd}}$  distribution of the black holes in our sample.

In Figure 2 we show the radio luminosity versus the black hole mass for objects of different spectral classes. Panel (a) shows the whole sample, while panel (b) concentrates on the SMBH only.

Overplotted are some of the linear regression fits discussed in the recent literature (see §3 for details).

Finally, Figure 3 shows the core radio luminosity versus the nuclear X-ray luminosity in the 2-10 keV band (left panel) and versus the ratio of the X-ray nuclear luminosity to the Eddington luminosity (right panel). We represent objects in different mass bins with different colors to highlight a possible segregation of different mass bins in the  $L_R - L_X$  plane.

In the next section we present a more quantitative statistical analysis of the correlations among  $L_R$ ,  $L_X$ , and  $M$ .

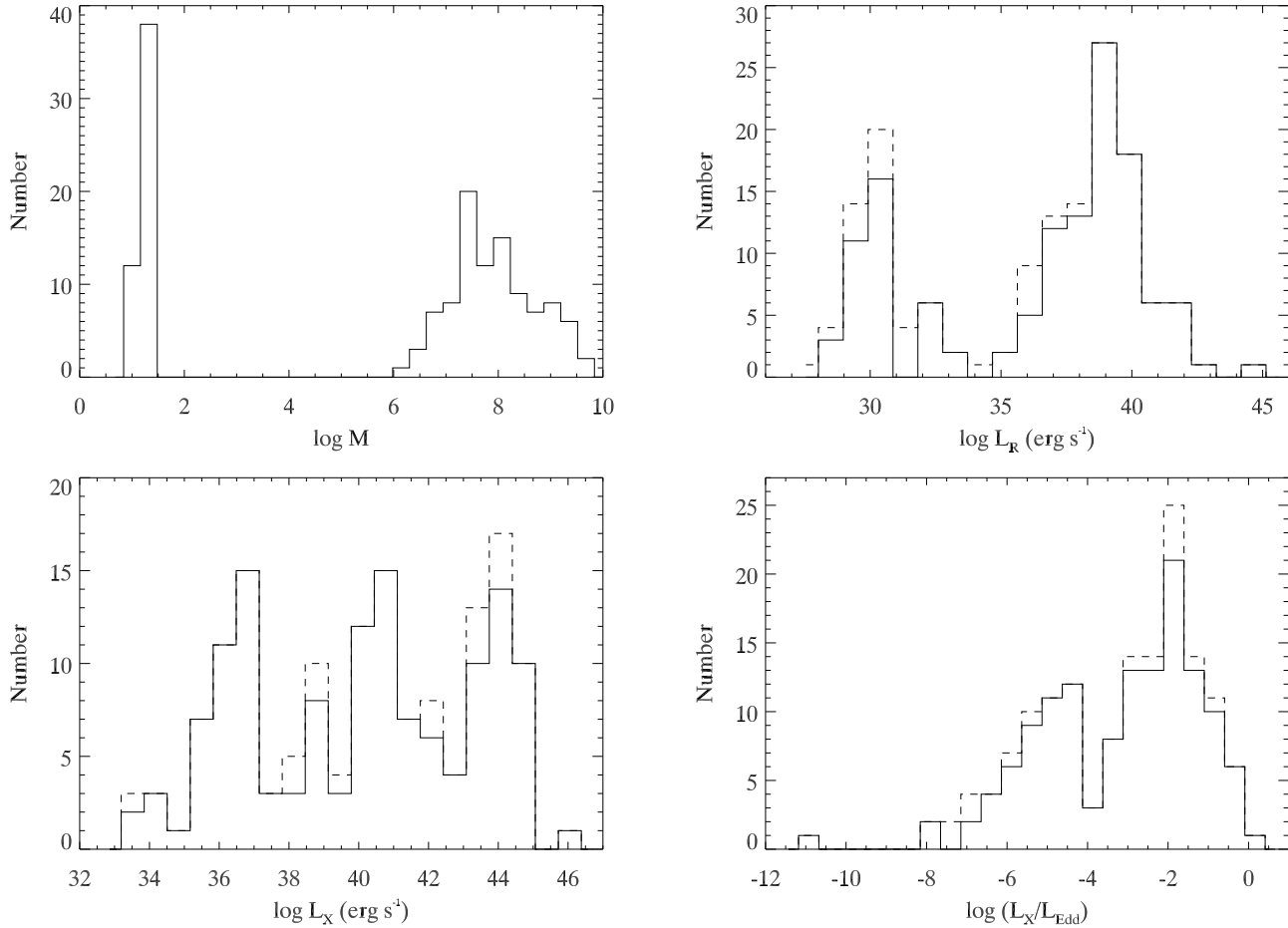


**Figure 1.** Distribution of black hole masses (top left panel), 5 GHz radio luminosity ( $L_R$ , top right panel), 2-10 keV X-ray luminosity ( $L_X$ , bottom right panel) and of the ratio  $L_X/L_{\text{Edd}}$ . Solid histograms denote detected sources, dashed ones are for upper limits.

### 3 CORRELATION ANALYSIS

Luminosity-luminosity correlations have to be tested for possible spurious effects introduced by their common dependence on the distance. Such tests can be done by performing a partial correlation analysis, taking distance as the third variable. Here we choose the so-called partial Kendall's  $\tau$  correlation test, proposed by Akritas & Seibert (1996) in the case of censored data sets. Applying this test to our data, we find that the  $L_R - L_X$  correlation is strong: the probability of the null hypothesis (i.e. that there is no correlation) is less than  $10^{-10}$  for the whole sample and  $\sim 1.12 \times 10^{-4}$  for the SMBH only (see Table 2).

However, it is apparent from Fig. 3 that, when the data points are grouped into mass bins, objects in different bins tend to lie on parallel tracks. Such a behavior can be seen both in the  $L_R - L_X$  plane (panel a), and, perhaps even more clearly, in the  $L_R - L_X/M$  plane (panel b). The presence of a mass segregation suggests that the radio luminosity of an object likely depends both on its X-ray luminosity and on its mass. In order to assess this hypothesis we once again use partial correlation analysis, now taking  $L_R$  (or  $L_X$ ) as the dependent variable and testing its partial correlation with  $L_X$  ( $L_R$ ) where we take  $M$  as the third variable. In addition, we also look for a partial correlation between  $L_R$  ( $L_X$ ) with mass itself, by taking  $L_X$  ( $L_R$ ) as the third variable. In so doing we can effectively

discriminate between intrinsic and spurious correlations among the three quantities.

The results of such tests (see Table 2) show that the radio luminosity is strongly correlated with both black hole mass and X-ray luminosity ( $P_{\text{null}} < 1 \times 10^{-10}$  for the whole data set), while in turn, the X-ray luminosity correlates with both mass and radio luminosity only if we include both GBH and SMBH ( $P_{\text{null}} \simeq 4.68 \times 10^{-5}$ ). These results imply that any regression fit used to find correlations between any two variables that does not account for the dependence on the third one (as, for example trying to find the dependence of  $L_R$  on  $M$  without accounting for the dependence on  $L_X$ ), inevitably leads to an incorrect estimate of the correlation coefficients.

If, in any case, we compute the correlation coefficients between any two of these variables<sup>2</sup> to allow a comparison with earlier works, we find that  $\log L_R^{\text{SMBH}} = (29.54 \pm 1.60) + (1.23 \pm 0.20) \log M$ , with a very large scatter (standard deviation  $\sigma_{\text{RM}}^{\text{SMBH}} = 1.65$ ). Including GBH, we find  $\log L_R^{\text{all}} = (28.75 \pm 0.18) + (1.20 \pm 0.04) \log M$  (standard deviation  $\sigma_{\text{RM}}^{\text{all}} = 1.51$ ), which is indeed very similar to what found by Nagar et al. (2002),

<sup>2</sup> We use a the linear regression method by parametric EM algorithm (that deals with censored data) as implemented in the ASURV package (Isobe, Feigelson, & Nelson 1986)

but very different from what was proposed by Franceschini et al. (1998), based on a much smaller sample (as shown by the different linear regression fits plotted in Figure 2).

We emphasize, however, that the partial correlation analysis presented so far and summarized in Table 2, implies that a far better representation of the mutual dependencies of  $L_R$ ,  $L_X$  and  $M$  (and the one that minimizes the scatter) should be searched for with multivariate linear regression tests, that allow simultaneous fitting over the 3-dimensional space defined by the three variables.

### 3.1 Finding the multivariate correlation coefficients

The standard multivariate regression formalism does not treat dependent and independent variables symmetrically (see, e.g., Fasano & Vio 1988). In other words, if a linear regression analysis yields a linear regression coefficient  $b$  for the dependence of  $y$  on  $x$ , it does not necessarily yield a coefficient  $b^{-1}$  for the dependence of  $x$  on  $y$ . Closely related to this is the fact that standard  $\chi^2$  statistics, for which errors are only associated with the dependent variable, artificially reduce the estimate of the correlation coefficient in the presence of intrinsic scatter in the independent variable. The net result of these shortcomings is that  $\chi^2$  distributions over the fitting parameter space are not fair representations of the confidence in the resulting best fit.

In order to alleviate these shortcomings, we extend the statistical approach used by the “Nukers” group (Gebhardt et al. 2000; Tremaine et al. 2002) to obtain an unbiased estimator of the best fit regression coefficients in multivariate problems. This approach uses a modified chisquare estimator, called the merit function (Fasano & Vio 1988; Press et al. 1992; Tremaine et al. 2002), defined by

$$\hat{\chi}^2 = \sum_i \frac{(y_i - a - \sum_j b_j x_{ij})^2}{\sigma_{y_i}^2 + \sum_j (b_j \sigma_{x_{ij}})^2} \quad (1)$$

where  $y_i$  is the dependent variable,  $x_{ij}$  are the independent variables and  $\sigma_{y_i}$  and  $\sigma_{x_{ij}}$  the associated error estimates,  $a$  is the zero intercept, and  $b$  are the linear regression coefficients, which are to be found. The argument of the sum in eq. (1) is a measure of the projected distance of the data point  $P_i = (x_{ij}, y_i)$  to the regression hyperplane given by the equation  $y = a + \sum_j b_j x_{ij}$ , measured in the  $\chi^2$  space around point  $P_i$ . In other words, the argument of the sum in eq. (1) counts the number of  $\chi^2$  intervals between  $P_i$  and the regression hyperplane. Because eq. (1) is nonlinear in  $b_j$ , it is no longer possible to minimize  $\hat{\chi}^2$  analytically. However, for a set of parameters  $b$ , we can still find the optimal value  $a_{\min}(b)$  for which  $\hat{\chi}^2$  is minimized as

$$a_{\min}(b) = \frac{\sum_i \frac{(y_i - \sum_j b_j x_{ij})}{\sigma_{y_i}^2 + \sum_j (b_j \sigma_{x_{ij}})^2}}{\sum_i \left( \sigma_{y_i}^2 + \sum_j (b_j \sigma_{x_{ij}})^2 \right)^{-1}} \quad (2)$$

Finding the best fit parameters is then a simple minimization problem which can be treated with standard numerical minimization routines. Because our analysis is restricted to a bivariate problem in this paper, it is possible to use a graphical solution in the form of 2-D  $\hat{\chi}^2$  contour plots.

Unfortunately, such a technique cannot handle censored data. However, it is easy to verify that the incidence of the censored data points in our sample on the estimate of the linear regression coefficient is small compared to the intrinsic scatter in the data. In order to do so, we have performed standard linear regression fit using

specific techniques that are able to handle censored data, as implemented in the ASURV package (Isobe, Feigelson, & Nelson 1986), on the whole data sample both with and without the upper limits. The differences in the resulting multivariate linear correlation coefficients in the two cases are much smaller than the estimated errors.

In the limit of  $\sigma_{y_i} \gg \sigma_{x_{ij}}$ , the merit function in eq. (1) recovers the traditional  $\chi^2$  estimator. This implies that the usefulness of eq. (1) is limited to cases where the estimated errors are an accurate representation of the true intrinsic uncertainty, including intrinsic scatter. Artificially large errors in one variable will introduce an asymmetry similar to that intrinsic to the traditional regression formalism. At face value, the errors in our sample are dominated by the uncertainties in the mass measurements. However, because we are using a sample of predominantly low redshift low luminosity AGN, error in the distance measurements can be large due to peculiar velocities, which leads to large errors in the luminosity measurements as well. For Galactic sources, distance estimates typically carry even larger uncertainties. Worse yet, the resulting errors in  $L_X$  and  $L_R$  will be correlated. As a first step, we therefore decided to follow the Nuker approach and assume isotropic uncertainties  $\sigma_{M_i} = \sigma_{L_{X,i}} = \sigma_{L_{R,i}}$  in all three variables and re-normalize these errors to produce a minimum reduced  $\hat{\chi}^2_{\text{red}} = \hat{\chi}^2/n_{\text{dof}}$  of unity.

## 4 RESULTS

We fit the data with the function

$$\log L_R = \xi_{RX} \log L_X + \xi_{RM} \log M + b_R, \quad (3)$$

or, alternatively with its reciprocal

$$\log L_X = \xi_{XR} \log L_R + \xi_{XM} \log M + b_X, \quad (4)$$

where we have used the merit function to estimate the best fit linear regression coefficients. Because the regression technique we adopt is symmetric<sup>3</sup>, eqs. (3) and (4) contain the same amount of information.

Our final results of the multivariate regression analysis are shown in the form of  $\chi^2$  contour plots (using eq. (1) as a  $\chi^2$  estimator) in the  $(\xi_{RM}, \xi_{RX})$  parameter space in Fig. 5. The top panel shows the results of the multivariate fit performed on the entire data set. We obtain  $\xi_{RX} = 0.60 \pm 0.11$ ,  $\xi_{RM} = 0.78^{+0.11}_{-0.09}$ , and  $b_R = 7.33^{+4.05}_{-4.07}$  (all the errors are one sigma confidence), with a dispersion  $\sigma_R = 0.88$ .

Our data set provides fairly tight constraints on the values of the correlation coefficients  $\xi_{ij}$  ( $i, j = R, X, M$ ). This in turn implies that in the 3-dimensional space  $(\log L_R, \log L_X, \log M)$  the sources are distributed preferentially on a plane, that we call hereafter the “fundamental plane” describing black hole activity. Figure 4 shows an edge-on view of the plane.

The other two panels of Fig. 5 show the constraints on the two correlation coefficients obtained with the regression analysis on different subsamples assembled according to the spectral properties in the radio band. For flat spectrum radio sources we obtain  $\xi_{RX,f} = 0.76 \pm 0.13$ ,  $\xi_{RM,f} = 0.71 \pm 0.10$ , and  $b_{R,f} = 1.31^{+4.85}_{-5.07}$ , with a dispersion  $\sigma_{R,f} = 0.81$ , smaller than that of the whole data set. The

<sup>3</sup> We verified that the standard regression technique is instead not symmetric: for the same fitting function (3), the best fit parameters are  $\xi_{RX} = 0.57$  and  $\xi_{RM} = 0.77$ , while by fitting eq. (4) we obtain  $\xi_{XR} = 1.05$  and  $\xi_{XM} = -0.49$ , instead of the expected  $\xi_{XR} = 1/\xi_{RX} = 1.75$  and  $\xi_{XM} = -\xi_{RM}/\xi_{RX} = -1.35$ .

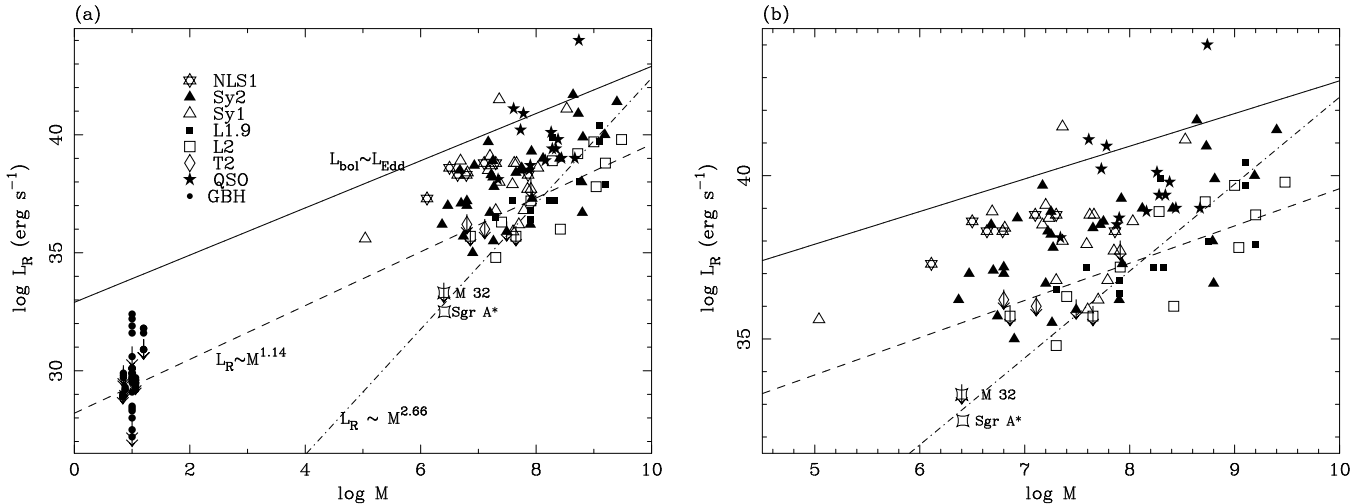


**Figure 2.** Radio core luminosity at 5 GHz versus black hole mass. Upper limits are marked with arrows. Panel (a) shows the whole sample, including GBH (black filled circles) and SMBH, with different symbols indicating objects belonging to different spectral classes. The right panel (b) is a blow up of the SMBH sample. The dot-dashed line gives the regression fit proposed by Franceschini et al. (1998), the dashed line that proposed by Nagar et al. (2002), both obtained using different samples of SMBH only. The thick solid upper line gives the maximum core radio power as calculated by Ho (2001) for sources accreting at the Eddington rate. Although a correlation analysis of our sample would give results similar to those obtained by Nagar et al. (2002), as we discuss in the text, *none* of the above relations reflects the real physical scaling of radio power and black hole mass.

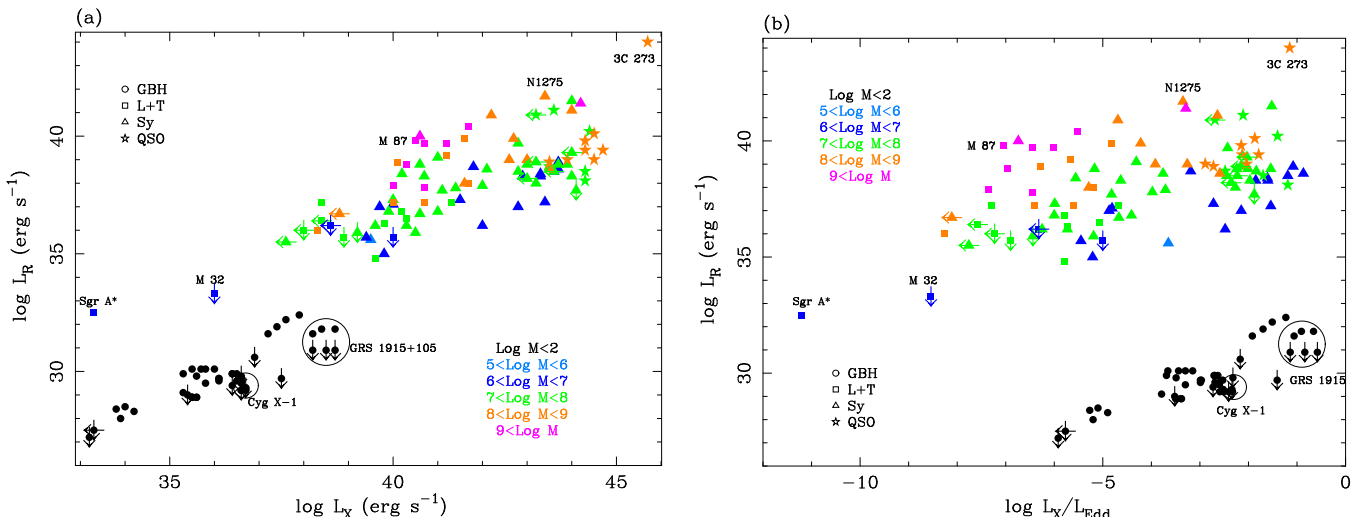


**Figure 3.** Radio core luminosity at 5 GHz versus X-ray luminosity in the 2-10 keV band (a) for the whole sample. Different colors correspond to different mass bins, while different symbols correspond to different classes of objects. In panel (b) we plot the same radio core luminosity at 5GHz vs. the ratio  $L_X/L_{\text{Edd}}$  of X-ray to Eddington luminosity. The color-coding of the different mass bins makes the mass segregation more evident.

difference in the coefficient for the  $L_R - L_X$  correlation with respect to the whole sample result may be due to a larger incidence of GBH in the flat spectrum subsample, which seem to have a slightly larger measured value of  $\xi_{RX}$  (Gallo, Fender, & Pooley 2002); the constraints on the other coefficient,  $\xi_{RM}$  are almost as good as for the entire data set, and in very good agreement with it.

On the other hand, in our steep spectrum sources subsample, only one GBH is included (LS 5039), and this results in a much larger uncertainty, in particular on the radio luminosity-mass correlation coefficient: ( $\xi_{RX,s} = 0.41^{+0.16}_{-0.18}$ ,  $\xi_{RM,s} = 0.94^{+0.21}_{-0.19}$ ,  $b_{R,s} = 14.08^{+5.92}_{-6.31}$  with dispersion  $\sigma_{R,s} = 0.87$ ).

## 5 PHYSICAL INTERPRETATION

As stated in the introduction, a correlation between X-ray and radio emission is expected if there is a fundamental connection between accretion flows and jet activity. Similarly, both the accretion flow properties and the jet emission must be somehow related with the black hole mass,  $M$ . At a qualitative level the existence the fundamental plane found in §4 is not surprising. However, in order to explore the physical implications of such a relationship and to constrain the physics of the inner accretion flow and of the inner jet, we now turn to a discussion of the theory of radio and X-ray emission by the jet-disc system.

**Table 2.** Results of Correlation analysis

Variables			Objects	Subsample				Correlation		
X (1)	Y (2)	Z (3)		N (5)	$N_{ul}^X$ (6)	$N_{ul}^Y$ (7)	$N_{ul}^Z$ (8)	$\tau$ (9)	$\sigma$ (10)	$P_{null}$ (11)
Log $L_R$	Log $L_X$	Log $D$	All Objects	149	20	14	0	0.255	0.0414	$7.3 \times 10^{-10}$
Log $L_R$	Log $L_X$	Log $D$	SMBH only	99	7	13	0	0.200	0.0518	$1.12 \times 10^{-4}$
Log $L_R$	Log $L_X$	$M$	All Objects	149	20	14	1	0.448	0.0495	$< 1 \times 10^{-10}$
Log $L_R$	Log $L_X$	$M$	SMBH only	99	7	13	1	0.450	0.0523	$< 1 \times 10^{-10}$
Log $L_R$	$M$	Log $L_X$	All Objects	149	20	1	14	0.432	0.0469	$< 1 \times 10^{-10}$
Log $L_R$	$M$	Log $L_X$	SMBH only	99	7	1	13	0.310	0.0547	$1.45 \times 10^{-8}$
Log $L_X$	$M$	Log $L_R$	All Objects	149	14	1	20	0.184	0.0452	$4.68 \times 10^{-5}$
Log $L_X$	$M$	Log $L_R$	SMBH only	99	13	1	7	-0.022	0.052	0.672

NOTE: Col. (1): Variable X. Col. (2): Variable Y. Col (3): Variable Z. Correlation between variables X and Y is studied, taking into account the mutual correlation of X and Y with Z. Col. (4): subsample. Col. (5): Number of objects in the subsample. Col. (6)-(8): Number of upper limits in X, Y and Z. Col. (9)-(11): Results of partial correlation analysis, giving the partial Kendall's  $\tau$  correlation coefficient, the square root of the calculated variance  $\sigma$ , and the associated probability  $P_{null}$  for accepting the null hypothesis that there is no correlation between X and Y.

## 5.1 Synchrotron emission from scale invariant jets

It was recently shown by Heinz & Sunyaev (2003) that the dependence of radio luminosity  $L_R$  on black hole mass  $M$  and dimensionless accretion rate  $\dot{m}$  can be cast into a model independent form *if the underlying jet physics is scale invariant*. In this case, all the model dependent uncertainties can be absorbed into the observable spectral index  $\alpha$ . The relationships between  $L_R$  and  $M$  and between  $L_R$  and  $\dot{m}$  depend only on the boundary conditions at the base of the jet, set by the conditions in the accretion flow feeding the jet. We will briefly review their argument (the interested reader is encouraged to consult Heinz & Sunyaev, 2003, for more details) before comparing their predictions to the correlations derived in the previous section.

The nature and conditions in the inner disc are most likely governed by only a few parameters ( $M$ ,  $\dot{m}$ , and possibly the black hole spin  $a$ ). The fundamental scale imposed on the problem is the gravitational radius of the black hole,  $R_g = GM_{\text{BH}}/c^2$ . Jet formation occurs in the innermost regions of accretion discs, thus it is natural that jet formation, too, is primarily governed by these three parameters only<sup>4</sup>.

The observational similarities between jets from SMBH and jets from GBH suggest that the process of jet formation and propagation is very similar, or, equivalently, that jet structure and dynamics are (at least approximately) invariant under changes of  $R_g \propto M$  and  $\dot{m}$ . In other words, taking a jet produced by a black hole of mass  $M_1$ , scaling its dimensions by a factor of  $M_2/M_1$  we should obtain a jet around a black hole of mass  $M_2$ .

This proposed invariance can be cast into a simple mathematical form. Any quantity  $f$  needed to calculate the synchrotron emission from jets can be decomposed into a structure function  $\psi_f(\mathbf{R}/R_g, a)$ , which describes the spatial variation of  $f$  along the jet, and which depends on  $M$  only through  $\mathbf{R}/R_g$ , and a normalization  $\phi_f(M, \dot{m}, a)$ , which is set by the boundary conditions at the base of the jet (thus, by accretion disc physics):

$$f(\mathbf{R}, M, \dot{m}, a) = \phi_f(M, \dot{m}, a) \cdot \psi_f(\mathbf{R}/R_g, a) \quad (5)$$

<sup>4</sup> The influence of  $a$  and the associated second scale of the problem, the light cylinder radius, on jet formation is unclear at this point. We will henceforth keep  $a$  fixed and assume that variations in  $a$  will only introduce a scatter in any relation derived below which is independent of  $M$  and  $\dot{m}$ .

The quantities necessary for calculating the jet synchrotron emission are the magnetic field strength  $B$ , the jet diameter  $D_{\text{jet}}$ , and the normalization  $C$  of the electron power-law distribution  $dn_e/d\gamma = C\gamma^{-p}$  (typically, the spectral index of the particle distribution is  $p \sim 2 - 3$ ). For example, according to the prescription (5), the magnetic field should follow  $B = \phi_B(M, \dot{m}, a) \cdot \psi_B(\mathbf{R}/R_g, a)$ , where  $\phi_B = B_0 = B(R_0)$  is the value of the field at the base of the jet  $R_0$ . As a geometric quantity, the jet diameter  $D$  should be directly proportional to the characteristic scale  $R_g$  such that  $\phi_D = D_0 = D(R_0) \propto R_g \propto M$ . Scale invariance also implies that dynamical time scales are proportional to  $R_g/c \propto M$ , and thus that characteristic velocities are scale invariant.

Using the standard formulae for synchrotron emission (Rybicki & Lightman 1979), Heinz & Sunyaev (2003) showed that the synchrotron luminosity  $L_\nu$  at a given frequency  $\nu$  emitted by the jet must then depend non-linearly on  $M$  and  $\dot{m}$ , following

$$\frac{\partial \ln(L_\nu)}{\partial \ln(M)} = \frac{2p + 13 + 2\alpha}{p + 4} + \frac{\partial \ln(\phi_B)}{\partial \ln(M)} \left( \frac{2p + 3 + \alpha p + 2\alpha}{p + 4} \right) + \frac{\partial \ln(\phi_C)}{\partial \ln(M)} \left( \frac{5 + 2\alpha}{p + 4} \right) \equiv \xi_M \quad (6)$$

and

$$\frac{\partial \ln(L_\nu)}{\partial \ln(\dot{m})} = \frac{\partial \ln(\phi_B)}{\partial \ln(\dot{m})} \left( \frac{2p + 3 + \alpha(p + 2)}{p + 4} \right) + \frac{\partial \ln(\phi_C)}{\partial \ln(\dot{m})} \left( \frac{5 + 2\alpha}{p + 4} \right) \equiv \xi_{\dot{m}} \quad (7)$$

where  $\alpha$  is the spectral index at frequency  $\nu$ .

The model dependent structure functions  $\psi_f(\mathbf{R}/R_g, a)$  scale out from these expressions. Only the spectral indices ( $\alpha$  and  $p$ ) and the boundary conditions  $\phi_B$  and  $\phi_C$  for the magnetic field  $B$  and the electron power-law distribution normalization  $C$ , respectively, remain.  $\alpha$  and  $p$  are observables: the electron spectral index  $p$  can be deduced from the optically thin synchrotron spectral index at high frequencies. The functions  $\phi_B$  and  $\phi_C$ , on the other hand, need to be provided by accretion disc theory. It is reasonable to assume that the relativistic particle pressure at the injection radius is a fixed fraction (i.e., independent of  $M$  and  $\dot{m}$ ) of the total pressure at injection,  $\phi_C \propto \phi_B^2$ . This leaves  $\phi_B$  as the only model dependent

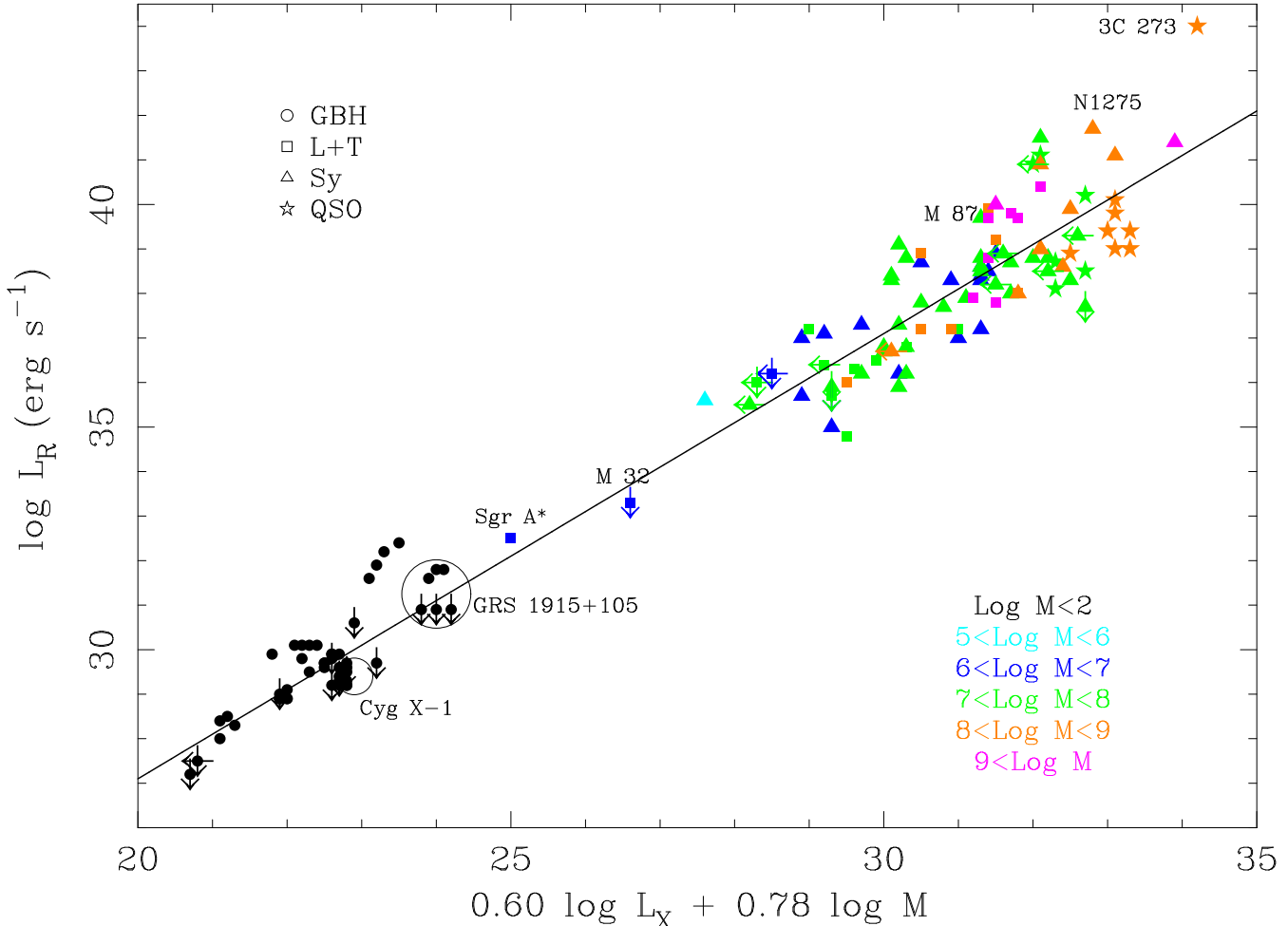


Figure 4. The edge-on view of the “fundamental plane of black hole activity”. The solid line shows the best fitting function (13).

parameter of the theory. Given a prescription for  $\phi_B$ , we can predict how the synchrotron luminosity of jets should scale with  $M$  and  $\dot{m}$ .

Since  $\xi_M$  and  $\xi_{\dot{m}}$  are constants, we have in general (with  $L_\nu = L_{5 \text{ GHz}} = L_R$ )

$$\log L_R = \xi_M \log M + \xi_{\dot{m}} \log \dot{m} + K_1, \quad (8)$$

where  $K_1$  is a normalization constant<sup>5</sup>. Variations in other parameters, such as the viewing angle or the black hole spin, will only introduce a scatter in this relationship that is *independent* of  $M$  and  $\dot{m}$ .

Because the expressions for  $\xi_M$  and  $\xi_{\dot{m}}$  do not depend on the shape functions  $\psi_f$ , they are independent of the model details. Any scale-invariant jet model that reproduces the observed radio spectral index  $\alpha_R$  *must* satisfy eqs. (6) and (7). This implies that (a) measurements of  $\xi_M$  and  $\xi_{\dot{m}}$  *cannot* be used to constrain the functions  $\psi_f$ , i.e., they cannot be used to distinguish between different jet models but that (b) measurements of  $\xi_M$  and  $\xi_{\dot{m}}$  *can* be used to

place constraints on the boundary conditions at the base of the jet  $\phi_f$ , or in other words on the accretion disc model.

While the black hole mass  $M$  is observable (see above), the accretion rate  $\dot{m}$  can only be inferred through radiation in other bands, where the emission is dominated by the accretion disc. Thus, in addition to a prescription of the boundary conditions  $\phi_f$  through accretion disc theory, we must also provide a relation between the accretion disc luminosity (or  $L_X$ ) and  $\dot{m}$  in order to model the observed  $L_R$ - $\dot{m}$  correlation. We must therefore discuss the different possible sources of the X-ray emission. We will start with those models that describe X-ray emission as produced by an accretion flow of some kind.

## 5.2 Accretion flow origin of X-ray radiation

For the accretion powered X-ray luminosity we can write, in analogy to eq. (8):

$$\log L_X = \log M + q \log \dot{m} + K_2 \quad (9)$$

where  $K_2$  is a normalization constant. The efficiency coefficient  $q$  need not be constant, though the linear correlation analysis from §3 is limited to this case.

Using eqs. (6-8) together with eq. (9), we obtain the following general expression for the *observable* correlation coefficients

<sup>5</sup> We note here that for flat spectrum jets with  $\alpha_R \sim 0$ , the canonical value of  $p \sim 2$ , and  $\phi_B^2 \propto M^{-1} \dot{m}$ , the dependence of  $L_R$  on  $M$  and  $\dot{m}$  follows  $L_R \propto (M \dot{m})^{17/12} = \dot{M}^{17/12}$ , as had been found by Falcke & Biermann (1996) for the specific case of the “canonical conical” (Blandford & Königl 1979) jet model.

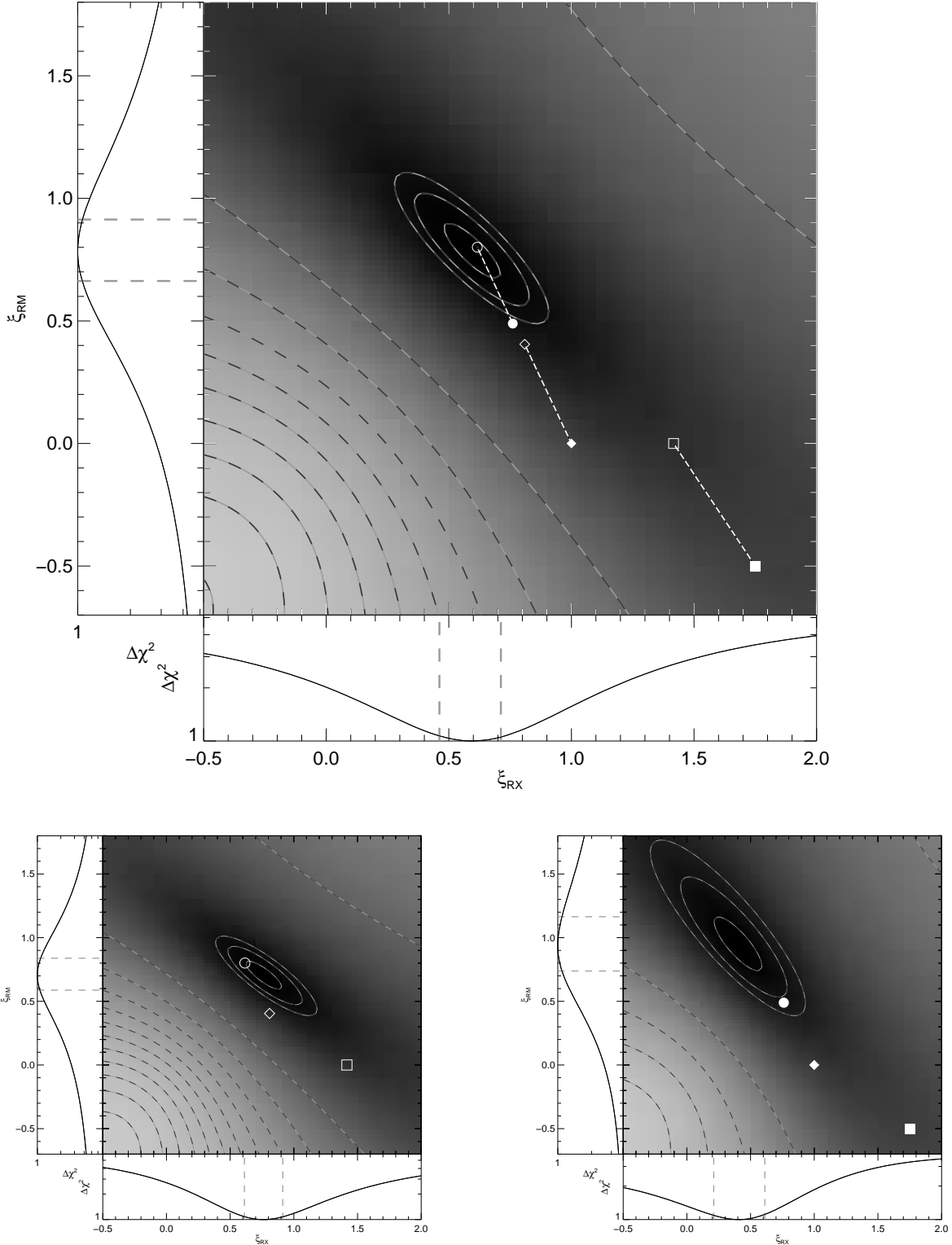


**Figure 5.** Shaded areas show the  $\chi^2$  density distribution, and dashed lines the  $\chi^2$  contours for the observed correlation coefficients  $\xi_{RM}$  and  $\xi_{RX}$ . The inner 3 contours show the formal 1,2 and 3 sigma confidence levels, the remaining contours further out show levels of  $\Delta\chi^2_{red} = 10$ . Shown are the results for: the entire data set (upper panel), the flat spectrum sources (lower left panel), the steep spectrum sources (lower right panel). Overplotted on each panel are the theoretically predicted values of the correlation coefficients where circles, diamonds and squares represent the ADAF, jet and standard disc models respectively. Empty symbols show the values for  $\alpha_R = 0$  and filled ones for  $\alpha_R = 0.5$ . The lines connecting the points represent the tracks of  $\xi_{RX}$  and  $\xi_{RM}$  traced out by variation of  $\alpha_R$ .

as defined in eqs. (3) and (4):

$$\begin{aligned}\xi_{RM} &= \frac{2p + 13 + 2\alpha_R}{p + 4} + \frac{\partial \ln \phi_B}{\partial \ln M} \left( \frac{2p + 13 + \alpha_R p + 6\alpha_R}{p + 4} \right) \\ &- \frac{\partial \ln \phi_B}{\partial \ln \dot{m}} \left( \frac{2p + 13 + \alpha_R p + 6\alpha_R}{q(p + 4)} \right) \\ \xi_{RX} &= \frac{\partial \ln \phi_B}{\partial \ln \dot{m}} \left( \frac{2p + 13 + \alpha_R p + 6\alpha_R}{q(p + 4)} \right).\end{aligned}\quad (10)$$

Different accretion models imply different values of  $q$ , and different scalings of the magnetic energy density at the base of the jet  $\phi_B$  with  $M$  and  $\dot{m}$ , resulting in different values of  $\partial \ln \phi_B / \partial \ln M$  and  $\partial \ln \phi_B / \partial \ln \dot{m}$ . We shall explore such models in the following sections.

### 5.2.1 Standard Shakura-Sunyaev discs coupled with a hot corona

In the standard Shakura-Sunyaev disc model (Shakura & Sunyaev 1973) accretion occurs via an optically-thick and geometrically thin disc. The effective optical depth in the disc is very high and photons are close to thermal equilibrium with electrons. The emission results in multi-color ( $T \propto M^{-1/2} r^{-3/4}$ ) blackbody spectrum. This component is thought to explain the “blue bump” in AGN and the soft X-ray emission in GBH. However, the standard model does not predict the power-law X-ray emission observed in all sub-Eddington accreting black holes.

It is generally accepted that the hard emission is produced by inverse Compton scattering of the soft, blackbody disc photons on a population of hot electrons that surround the cooler disc in the innermost region of the accretion flow (the so-called *corona*). In these models a fraction  $f_c$  of the gravitational power is dissipated in the corona (and eventually emerges as X-ray radiation). The X-ray luminosity can then be written as  $L_X \sim f_c \dot{m} L_{\text{Edd}} \propto f_c \dot{m} M$ , and the coronal magnetic energy density follows  $B^2 \propto \dot{m} f_c / M$  (e.g.; Haardt & Maraschi 1991; Di Matteo, Celotti & Fabian 1999; Merloni & Fabian 2002).  $L_X$  should therefore scale linearly with  $\dot{m}$ , as long as the fraction of power dissipated into the corona  $f_c$  does not change with the accretion rate.

In order to confirm this, we have calculated the expected spectral energy distributions for a typical disc-corona accretion system around a  $10M_\odot$  black hole, with constant  $f_c$  ( $\sim 0.8$ ) and  $\dot{m}$  ranging from  $10^{-6}$  to 0.1 (we have assumed here  $\dot{M}_{\text{Edd}} = 10L_{\text{Edd}}/c^2 = 2.2 \times 10^{-8} M M_\odot \text{ yr}^{-1}$ , i.e., a canonical 10% efficiency). The spectra, shown in the top panel of Fig. 6, are composed of a multicolor blackbody Compton scattered by a corona with a fixed Thompson scattering optical depth  $\tau = 0.5$  and temperature,  $kT = 100 \text{ keV}$ , which are typical values deduced from X-ray spectra of GBH (and AGN) and a reflection component due to scattering of hard X-ray photons back in the disc for a corona covering an angle of  $\pi/2$  of the disc (the details of the spectral model are described by Di Matteo et al. 1999). In such models (bottom panel of Figure 6),  $L_{2-10 \text{ keV}} \propto \dot{m}$  as expected from the simple energetic scalings above. Note, however, that we expect some scatter in this relation due to intrinsic changes in the coronal plasma optical depth and temperature that may have some dependence on the accretion rate.

Merloni & Fabian (2002) and Merloni (2003) have shown how it is possible to derive coupled equations for the accretion disc-corona systems under very simple assumptions about the nature of the turbulent magnetic viscosity inside the disc. The main property of their self-consistent coupled treatment is that  $f_c$  is indeed constant when gas pressure dominates in the disc, so for accretion

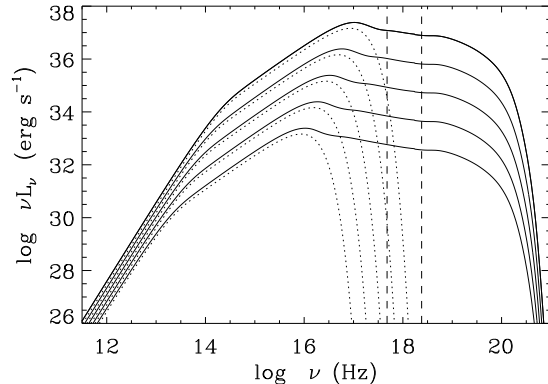


**Figure 6.** Predictions from a disc-corona model for  $\dot{m} = 10^{-6}, 10^{-5}, 10^{-4}, 10^{-3}, 0.01, 0.1$ . The total broad band spectral energy distributions include a multicolor blackbody spectrum (dotted lines) Compton scattered by a corona with fixed  $\tau = 0.5$  and  $kT = 100 \text{ keV}$ . The resulting reflection component is also calculated. The dashed lines show the  $2 - 10 \text{ keV}$  energy band.

rates  $\dot{m} \lesssim 0.016(\alpha_v M)^{-1/8}(1 - 0.84\alpha_v^2)^{-9/8}$  (with  $\alpha_v$  viscosity parameter), while  $f_c \propto \dot{m}^{-1/2}$  in the radiation pressure dominated parts of the disc. In accordance with the above scenario, the scaling indices for the disc-corona case are written in Table 3. It is worth noting that  $q$  and  $\partial \phi_B / \partial \dot{m}$  enter eq. (10) in such a way that the correlation coefficients  $\xi_{RM}$  and  $\xi_{RX}$  are identical for the gas and radiation pressure dominated disc cases.

### 5.2.2 Non radiative accretion flows

The standard solution we have discussed in the previous section is not a unique solution for the accretion flow equations at low accretion rates. In recent years, much work has been devoted to the detailed study of low radiative efficiency accretion and in particular to the so called Advection Dominated Accretion Flows (ADAF) solutions (Narayan & Yi 1994; Narayan & Yi 1995; Abramowicz et al. 1995; Narayan, Mahadevan, & Quataert 1998). The latter usually refers to the optically-thin ADAF branch which is established only for accretion rates lower than a critical value  $\dot{m} < \dot{m}_{\text{crit}} \sim \alpha_v^2$  (Rees et al. 1982). It is worth noting that from both the theoretical point of view (Narayan, Igumenschev, & Abramowicz 2000) and from numerical simulations (Igumenschev & Abramowicz 2000; Hawley & Balbus 2002), it has been shown that that radiatively inefficient flows are prone to strong convective instabilities and/or powerful outflows which alter the nature of the solutions significantly. Despite the extensive theoretical efforts, however, the relative importance of convection and outflow for adiabatic flows is still a matter of significant debate (Balbus & Hawley 2002; Narayan et al. 2002) and no strong observational discriminant has yet been found.

Indeed, mass accretion via radiatively inefficient accretion flows (ADAF in particular) have been fairly successfully invoked to explain the spectral states of GBHs (Narayan, Garcia, & McClintock 1997; Esin, McClintock, & Narayan 1997) and shown to be consistent with observations of low luminosity AGN (Narayan et al. 1998a;

Quataert et al. 1999; Di Matteo et al. 2000; Di Matteo et al. 2003). For the GBH models, the accretion flow is typically divided into two distinct zones. The inner part is modeled as hot optically thin ADAF while the outer part consists of an optically thick standard thin disc. The transition from the hard to the soft state of GBHs is assumed to occur as the geometrically thin disc moves inwards and most of the dissipated energy emerges in the form of a blackbody-like spectrum.

From our point of view, it is important not only to understand how the value of the magnetic field in such flow scales with  $M$  and  $\dot{m}$ , but also to have a detailed model for their radiative output, in order to predict the scaling of the X-ray emission with these parameters. From general arguments, we expect any mechanically cooled flow to obey  $\phi_B^2 \propto M^{-1}\dot{m}$  (Heinz & Sunyaev 2003). On the other hand, the exact value of  $q$  can only be determined once a detailed assessment of the radiative processes that give rise to observed luminosity is made. This is what we discuss in the following, in the framework of the ADAF model, which is the only one for which detailed spectral modeling has been done so far.

A hot accretion flow around a stellar mass (supermassive) black hole radiates mostly in the optical (radio) to X-ray bands. In the optical (radio) band, the emission results from synchrotron radiation. At higher energies, and up to the X-ray band, the emission is produced by bremsstrahlung processes for low accretion rates and inverse Compton scattering of the soft synchrotron photons or blackbody photons from the disc in the outer regions when the accretion rate approaches the critical value (Narayan, Barrett, & McClintock 1998). The predicted spectrum from an ADAF depends (weakly) on the ratio of the gas to magnetic pressure  $\beta$ , the viscosity parameter  $\alpha_v$ , and the fraction of the turbulent energy in the plasma which heats the electrons,  $\delta$ . Here, we fix  $\alpha_v = 0.1$ ,  $\beta = 10$ , and take  $\delta = 0.3$ .

The top panel of Figure 7 shows the spectra of ADAFs (plus outer thin disc for  $\dot{m} \sim \dot{m}_{crit}$ ) for ten accretion rate values starting from  $\dot{m} = 10^{-6}$  up to  $\dot{m} \sim \dot{m}_{crit} \sim 10^{-2}$ . The middle panel shows the relationship between the 2–10 keV luminosity,  $L_X$ , and both the accretion rate,  $\dot{m}$  (for  $M = 10$ , top panel) and the mass,  $M$  (for a fixed  $\dot{m} = 0.01$ , bottom panel). For the chosen values of the parameters  $\alpha_v$ ,  $\beta$  and  $\delta$ , the dependence of the 2–10 keV luminosity on  $\dot{m}$  is roughly given by:

$$L_{X,2-10\text{keV}} \propto \begin{cases} \dot{m}^{3.4}, & \dot{m} \lesssim 10^{-4} \\ \dot{m}^{1.6}, & 10^{-4} \lesssim \dot{m} \lesssim 5 \times 10^{-3} \\ \dot{m}^2, & 5 \times 10^{-3} \lesssim \dot{m} \lesssim 2 \times 10^{-2} \end{cases} \quad (11)$$

The full band spectra shown in Figure 7 with the two vertical lines indicating the 2–10 keV energy band illustrate the origin for the various dependences shown in equation (11). For  $\dot{m} \lesssim 10^{-4}$  the integrated 2–10 keV emission includes both the first order Comptonized component, which drops off at around few keV, and bremsstrahlung which dominates the emission at higher energies. At higher accretion rates the first (or higher) order Compton scattering of softer photons always dominate the 2–10 keV emission (see Figure 7, top panel). At these higher rates the optical depth increases and cooling becomes overall more efficient.

This can also be seen in middle panel of Figure 7, where we also plot (dashed line) the electron temperature at  $r = 3$  as a function of  $\dot{m}$ . The temperature is nearly constant for  $\dot{m} \lesssim 10^{-4}$ ; in this regime the viscous heating is virtually fully balanced by advection. At  $\dot{m} \gtrsim 10^{-4}$  cooling processes become more important and the temperature decreases. The overall change in the dependences in eq. (11) reflects this behavior.

However, it is important to keep in mind that the exact depen-

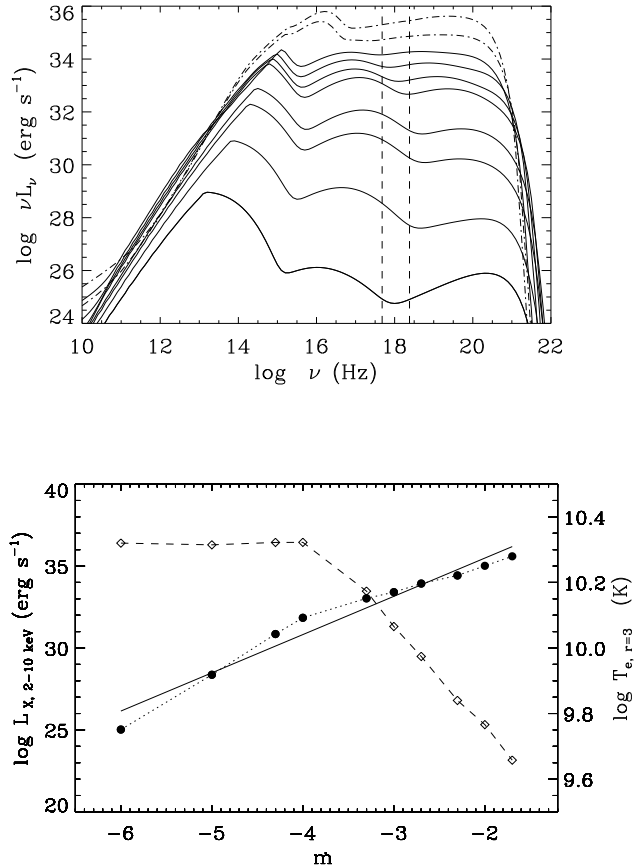


**Figure 7.** Predictions from ADAF models for  $\dot{m} = 10^{-6}, 10^{-5}, 5^{-5}, 10^{-4}, 5 \times 10^{-4}, 10^{-3}, 2 \times 10^{-3}, 5 \times 10^{-3}, 10^{-2}$ . The top panel shows the broad band spectral energy distributions for a fixed  $M = 10$ , with the vertical dashed lines enclosing the 2–10 keV spectral energy band. For the top two models (dot-dashed lines) we also plot the multicolor blackbody from an outer thin disc with an inner edge at  $r = 40$ . In the bottom panel: the solid dots joined by the dotted line show the integrated 2–10 keV X-ray luminosity and the open symbols joined by dashed lines and the flow electron temperature at  $r = 3$  versus the accretion rate  $\dot{m}$ . The solid line is a linear fit to the 2–10 keV luminosity over the whole of the  $\dot{m}$  with slope 2.3.

dences in this narrow band will also depend on the microphysical parameters that we choose for the model. For instance, variations in the electron heating parameter,  $\delta$  will result in changes in the Comptonization spectra. Therefore, in order to compare theoretical predictions with the observed data, the intrinsic scatter of which does not allow us to put tight constraints on the different emission regimes, we fit the  $L_X - \dot{m}$  relation over the whole range of  $\dot{m}$  and obtain a single power-law,  $L_X \propto \dot{m}^{2.3}$  (as shown by the solid line in the middle panel of Figure 7). We also calculate the relation between  $L_{2-10\text{keV}}$ , versus the black hole mass,  $M$  for the models and, as expected, the relation is very close to linear with  $L_X \propto M^{0.97}$ .

### 5.3 Jet origin of X-ray radiation

The presence of both high energy electrons and radio/optical radiation implies that the inner jet must emit inverse Compton X-rays,

**Table 3.** Scaling indices of the X-ray luminosity and of the magnetic field as functions of the physical parameters  $\dot{m}$  and  $M$  for different accretion flow models.

accretion model	$q$	$\frac{\partial \ln \phi_B}{\partial \ln M}$	$\frac{\partial \ln \phi_B}{\partial \ln \dot{m}}$
disc/corona, gas	1	-1/2	1/2
disc/corona, rad	1/2	-1/2	1/4
ADAF	2.3	-1/2	1/2
brehms. emission only	2	-1/2	1/2

contributing to the overall X-ray spectrum at some level. However, under suitable conditions even the synchrotron component will reach X-ray energies. Especially in the presence of relativistic beaming, synchrotron emission could actually be responsible for the bulk of the X-rays. It is therefore useful to discuss the radio-X-ray-mass correlation expected for the synchrotron X-ray scenario (Markoff, Falcke, & Fender 2001).

While at low frequencies the effects of synchrotron self-absorption lead to the flat spectrum typically observed in core dominated sources, at high frequencies the jet becomes optically thin to synchrotron self-absorption, following the well known optically thin power-law with X-ray spectral index  $\alpha_X = (p - 1)/2$ .

Because X-rays and radio emission now originate from the same source, it is straightforward to derive the relation between the two components. The correlation coefficients  $\xi_M$  and  $\xi_{\dot{m}}$  for the optically thick radio emission are still given by eqs. (6) and (7), while for the optically thin X-ray emission we can simply substitute  $\alpha_X = (p - 1)/2$  in those expressions. Finally, we can eliminate  $\log \dot{m}$  from eq. (8) in favor of  $\log L_X$  and arrive at the desired expressions for the correlation coefficients:

$$\begin{aligned} \xi_{RX} &= \frac{2(2p + 13 + \alpha_R p + 6\alpha_R)}{(p + 4)(p + 5)} \\ \xi_{RM} &= \frac{2p + 13 + 2\alpha_R}{p + 4} - \frac{6(2p + 13 + \alpha_R p + 6\alpha_R)}{(p + 4)(p + 5)} \end{aligned} \quad (12)$$

where  $\alpha_R$  is the radio spectral index and  $p$  is assumed to be the same for radio and X-ray emitting electrons<sup>6</sup>, and we have used a tilde to distinguish the synchrotron X-ray model.

#### 5.4 Comparison with observations

In the previous sections we have shown how different theoretical models for the emission processes responsible for the observed radio and X-ray emission from black holes can be directly translated into predictions for the observable correlation coefficients  $\xi_{RX}$  and  $\xi_{RM}$  (see eq. 3). The relatively tight observational constraints on these indices that we have derived in section 3 can therefore be used to directly test these models. The theoretical coefficients for different models are shown in Figure 5. The circles and the squares denote inefficient and efficient disc accretion respectively. Diamonds represent synchrotron X-rays from the jet. Open and closed symbols are for flat ( $\alpha_R = 0$ ) and steep ( $\alpha_R = 0.5$ ) spectrum sources, respectively. All model coefficients are calculated assuming  $p = 2$

<sup>6</sup> This implies that radiative cooling must either be negligible for the region of the jet where the X-rays are produced, leaving  $p \sim 2$  over the entire spectrum, or that cooling and continuous injection have produced a universal power-law with a slope of order  $p \sim 3$ . This limitation, while severe, cannot be avoided because particle transport including the effects of radiative cooling cannot be formulated in a simple scale invariant fashion.

(but see §6.3 for a discussion of steeper electron distributions as due, for example, to the effects of cooling). To highlight the sensitivity of the coefficients to variations in  $\alpha_R$ , we also plotted the tracks in  $\xi_{RX} - \xi_{RM}$  space for changes in  $\alpha_R$  between 0 and 0.5.

For the models in which X-rays are produced by inefficient accretion, we have  $q = 2.3$  and  $\partial \ln \phi_B / \partial \ln \dot{m} = -\partial \ln \phi_B / \partial \ln M = 0.5$  (see §5.2.2). The predicted coefficients for both flat and steep spectrum sources lie roughly within the  $3\sigma$  contours of the observed sample. Thus, inefficient accretion is consistent with the observations. We also considered a more general radiatively inefficient, mechanically cooled accretion model, where the X-ray luminosity is entirely produced by bremsstrahlung, for which we expect  $q = 2$ . While this moves the points further out of the central contours, this model is still consistent with the observations.

For the standard disc-corona model, we take  $q = 1$  (high radiative efficiency) and  $\partial \ln \phi_B / \partial \ln \dot{m} = -\partial \ln \phi_B / \partial \ln M = 0.5$  (see §5.2.1). The model predictions fall well outside the  $3\sigma$  contours of the data and are therefore inconsistent with the observations.

For the models in which the X-rays are produced by optically thin synchrotron emission from the jet itself, the flat spectrum model predictions are marginally consistent with the data (the model point is close to the  $3\sigma$  contour), while the steep spectrum model point lies well outside the  $3\sigma$  contour.

These results suggest that, in a statistical sense, the correlations between radio luminosity, X-ray luminosity and mass of active black holes are best explained by a radiatively inefficient accretion flow coupled with a (scale invariant) synchrotron emitting jet. This conclusion holds over the observed range of  $L_X / L_{\text{Edd}}$ , and therefore for sources which are substantially sub-Eddington. In §6.5 we discuss what should be expected from similar studies performed on samples that include a larger number of very luminous black holes.

The jet synchrotron model for the X-ray emission with  $p = 2$  is only marginally consistent with the data. However, steeper electron distributions ( $p = 3$ , for example) do predict values for the correlation coefficient that are well within our  $3\sigma$  contours. An assessment of the relevance of such models should be made taking in due account the effect of cooling, as we discuss in §6.3.

## 6 DISCUSSION

### 6.1 The thickness of the fundamental plane

The main result of our work is the discovery of a “fundamental plane” of black hole activity. That is, if we define the instantaneous state of activity of a black hole of mass  $M$  (in units of solar masses), by the radio luminosity at a fixed frequency (for example at 5 GHz), and by the hard X-ray luminosity (for example in the 2-10 keV energy band) of its compact core, and represent such an object as a point in the three-dimensional space ( $\log L_R, \log L_X, \log M$ ), all the points representing black holes (either of stellar mass or supermassive) will lie preferentially on a plane, described by the equation:

$$\log L_R = (0.60^{+0.11}_{-0.11}) \log L_X + (0.78^{+0.11}_{-0.09}) \log M + 7.33^{+4.05}_{-4.07} \quad (13)$$

We note that in the case the radiatively inefficient disc model ( $q = 2.3$ ) the fundamental plane equation (13) implies that the radio luminosity satisfies:

$$L_{R,q=2.3} \propto \dot{m}^{1.38} M^{1.38} = \dot{M}^{1.38}, \quad (14)$$

i.e.,  $L_R$  scales with the *physical accretion rate* only. This is very close to the predicted dependence of  $L_R \propto \dot{M}^{1.42}$  from 5.1 for the canonical parameter choice of  $\alpha = 0$ ,  $p = 2$ , and  $\phi_B \propto M^{-1/2}\dot{m}^{1/2}$ , for which the kinetic jet power  $W_{\text{jet}}$  is directly proportional to the physical accretion rate,  $W_{\text{jet}} \propto \dot{M}$  (see also Falcke & Biermann 1995).

The fundamental plane defined in eq. (13) is not, however, razor thin. The sources are substantially scattered around it, with a dispersion  $\sigma = 0.88$  in  $\log L_R$  (corresponding to a dispersion of  $\sigma_{\perp} = 0.62$  perpendicular to the plane). Such a scatter is not at all surprising. Theoretically, it can be explained in large part by the scatter in the radio spectral index  $\alpha_R$ . For example, if we consider the ADAF ( $q = 2.3$ ) model with fixed  $p = 2$ , we expect the theoretical relationship  $L_R = (0.62 + 0.29\alpha_R)\log L_X + (0.80 - 0.62\alpha_R)\log M + b_R$ . For the sake of simplicity, let us assume now that the unknown radio spectral index of all the observed sources is normally distributed, with  $\alpha_R = \langle \alpha_R \rangle \pm \sigma_{\alpha}$ . In order to fit the observed data, we need  $\langle \alpha_R \rangle \approx 0$  and  $b_R \approx 7$ . The dispersion in the radio luminosity due to the dispersion in the unknown parameter  $\alpha_R$  is then  $\sigma_R \gtrsim \sigma_{\alpha} \sqrt{0.33^2 (\Delta \log M)^2 + 0.29^2 (\Delta \log L_X/M)^2} \sim 2\sigma_{\alpha}$  where  $2\Delta \log M$  is the range in  $M$  and  $2\Delta \log L_X/M$  the range in luminosity spanned by our sample. Thus, a dispersion in the unknown radio spectral index of  $\approx 0.3$  (consistent with the observations), can give a large contribution to the observed intrinsic scatter.

In addition to the scatter produced by the diversity in  $\alpha_R$  (which introduces scatter in the fundamental plane relation simply by the fact the *orientation* of the plane is slightly different for different  $\alpha_R$ ) the *intercept*  $b_R$  of the plane also varies as we look at different jet models and different spectral indices. It is not clear a-priori how much it does so, as this depends on how the shape functions  $\psi_f$  (see section 5.1) vary in order to produce the different  $\alpha_R$ . While for one spectral class with uniform  $\alpha_R$  the normalization cancels out when determining the correlation coefficients, this is not true when comparing jets from different spectral classes, i.e., with varying  $\alpha_R$ . The fact that the scatter in the relation is moderate indicates, however, that the change in  $\psi_f$  over the range of radio spectral slopes that enter our sample is also moderate.

Ideally, we should therefore restrict the above analysis to sub-classes of sources which follow a very narrow range in  $\alpha_R$ . However, at the current stage the data do not allow such a division, both because the sample is too small and because the spectral indices are often not known to an accuracy that would allow such a treatment. The rough division of our sample into flat and steep spectrum sources nonetheless shows that such a treatment is possible and does lead to a reduction in scatter in the well defined and well sampled class of flat spectrum sources, for which we can be confident that the radio emission does indeed originate in the self-absorbed core of the jet (a prerequisite of the scale invariance model by Heinz & Sunyaev, 2003).

Other sources of scatter may well be present in our data set. In particular, the effects of relativistic beaming may be important for the most powerful radio sources. Already, the tightness of the  $L_R - L_X$  relation has inspired (Gallo, Fender, & Pooley 2002) to suggest that relativistic beaming is unimportant in Galactic sources in the low-hard state. Should the intrinsic scatter in a larger, carefully selected sample over the whole mass range with accurate spectral information be similarly low to that found in our sample, a similar conclusion could be reached about low luminosity AGNs.

Another source of scatter could be the influence of the black hole spin on jet formation. While we still expect the accretion disc to have significant influence on the jet power, as the magnetic field

necessary to tap the black hole rotational energy must be provided and/or confined by the accretion disc (thus setting the field strength and the jet power), the spin itself will enter as a sensitive parameter into the radio luminosity as well, introducing scatter in any correlation. Once again, strong future constraints on the tightness of this relation may help constrain the possible influence of black hole spin.

## 6.2 Steep spectrum sources

For the steep spectrum sources in our sample, the origin of the radio emission is not entirely clear. Steep spectra in general imply optically thin emission. This could be an indication that the emission is dominated by regions far away from the central engine, e.g. in the diffuse extended radio lobes or hot spots. This would prohibit any treatment that makes use of the scale invariant model, though scaling arguments for the large scale emission still apply (Heinz 2002). Steep spectrum sources should then be excluded from the sample completely, and the fact that they still fit into the plane would then mostly be due to selection effects. It should be noted that in this case the radio luminosity should strongly correlate with the black hole mass (which determines the kinetic jet power  $W_{\text{jet}}$  and thus the large scale radio luminosity), while it should not be related to the instantaneous X-ray flux, because the radio lobes reflect the mean power output by the central source, averaging out its temporal variability. We expect this to be a problem for Galactic black hole sources, where we have lower resolving power. For supermassive black holes and for nearby LLAGN in particular, we can be more confident that the large scale emission is well resolved and thus does not contribute to the core emission used in our sample.

It is also possible that some of the steep spectrum sources can be associated to core jet emission which is optically thin at radio frequencies, i.e., their self-absorption break lies below 5 GHz. Because we would expect the self-absorption break frequency to be lower for higher  $M$  and lower accretion rates  $\dot{m}$  (Heinz & Sunyaev 2003), this effect would imply that steep spectra should predominantly be observed in SMBH which are relatively X-ray dim. While the trend with  $L_X$  is not clear in the data, the fact that the steep spectrum sources in our sample almost exclusively belong to the SMBH class does suggest that at least some of the sources in the sample might indeed be core dominated steep spectrum sources, for which the theoretical analysis of §5 holds.

## 6.3 X-ray emission from jets

Our analysis, taken at face value, does suggest that accretion models for the origin of the X-ray emission fit the data somewhat better than pure jet models. However, at X-ray energies the effects of cooling on the particle spectrum cannot be ignored. In the context of scale invariant models, taking cooling into account is not possible. Proper treatment of particle transport including the effects of cooling may lead to different results for the synchrotron X-ray model. In fact, simply using  $p = 3$  in eq. (12) (as expected in a continuous particle injection model with cooling) moves the flat spectrum point close to the  $1\sigma$  contour of the observed correlation in Fig. 5.

For the case of the galactic black hole GX 339-4 in the hard state, where the radio-X-rays correlation is well established, Markoff et al. (2003) were able to fit the observed slope ( $\xi_{RX,339} \simeq 0.71$ ) with a synchrotron X-ray model assuming  $p = 2.15$  (and thus  $\alpha_X = 0.58$ , which is also close to the average slope of the X-ray spectral index of the source in the hard state). Here we have

shown that, in a statistical sense, higher values of  $p$  are probably needed to explain the observed correlation for the entire sample in the framework of the jet synchrotron model for the X-ray emission.

Furthermore, for  $p = 2$  the X-ray synchrotron luminosity from the jet scales like  $L_{X,\text{synch}} \propto M^{1.25}$ , while the disc X-ray luminosity follows  $L_{X,\text{disc}} \propto M$ . Thus, if the X-ray emission in GBH jets like GX 339-4 were indeed due to synchrotron emission, we would expect an even stronger contribution from synchrotron X-rays relative to the disc emission in AGNs with the same accretion rate, where the general wisdom (mainly based on accurate analysis of detailed X-ray spectra) is still that the X-rays originate predominantly in the disc. For  $p = 3$ , on the other hand, the synchrotron X-rays follow  $L_{X,\text{synch}} \propto M$ , and the relative contribution from jet and disc will be independent of  $M$ .

Finally, the X-ray spectral variability behaviour of both GBH and Seyfert galaxies is consistent with pivoting of the spectrum at X-ray energies. If the X-ray emission is produced by synchrotron radiation and there is no cooling break at longer wavelengths, such a power-law variability would imply a radio variability which is orders of magnitude larger than observed (see discussion in Zdziarski et al. 2003).

It seems, therefore, that if the X-ray emission in some of the sources is dominated by synchrotron emission from the jet, the effects of cooling must play an important role in determining the observed correlation. In the context of the scale-invariant model, it is rather problematic to take cooling into account; this is why a theoretical assessment of the role of the cooling on the observed correlation is beyond the scope of this paper.

#### 6.4 Estimating black holes masses and the nature of ULXs

Due to the intrinsic scatter, the predictive power of the  $\log M - \log L_X - \log L_R$  relation is currently limited in scope. Nonetheless, from the fundamental plane equation (13), we can derive a formal relationship between the observed fluxes in the radio (at 5 GHz) and in the X-ray (2-10 keV) band (in  $\text{erg s}^{-1} \text{cm}^{-2}$ ), the distance to a source  $D$  (in Mpc) and its unknown mass. We obtain

$$\log M \simeq 16.3 + \log D + 1.28(\log F_R - 0.60 \log F_X) \pm 1.06. \quad (15)$$

In particular, we can predict in which region of  $\log L_R - \log L_X$  space we would expect to find intermediate mass black holes, if they exist, and specifically, where we would expect Ultra-Luminous X-ray sources (ULX; Makishima et al. 2000) based on their X-ray flux, should they be intermediate mass black holes, as opposed to intrinsically beamed low mass black holes.

As an example, we refer to the recent claim of the observation of synchrotron radio emission from the ULX 2E 1400.2-4108, in the dwarf irregular galaxy NGC 5408 (at a distance of  $\sim 4.8$  Mpc) (Kaaret et al. 2003). The observed radio ( $0.26$  mJy at 4.8 GHz) and X-ray fluxes ( $2.7 \times 10^{-12}$   $\text{erg s}^{-1} \text{cm}^{-2}$  in the 0.3-8 keV band), if indeed both associated with a compact source at the distance of NGC 5408, would imply a mass of  $\log M \simeq 4 \pm 1$ . However, we should stress here that such an estimate only holds if the radio emission is not beamed. The uncomfortably high value for the estimated mass, the steep inferred radio spectral index and the radio to X-ray flux ratio, all suggest that the observed intensity of the radio emission may be Doppler boosted by a relativistic jet pointing in our direction (Kaaret et al. 2003).

#### 6.5 Accretion mode changes

It is well accepted, both from theory and observations, that accretion can proceed in different modes (or states), with different radiative efficiencies and spectral properties (Abramowicz 1998; Done 2002; Frank, King, & Raine 2002; Narayan 2002), mainly driven by variations of the dimensionless accretion rate  $\dot{m}$ . Here we have demonstrated (§5) that the correlation between radio and X-ray luminosity in GBHs and SMBHs can provide valuable constraints on the emission mechanisms in these bands and on the physics of accretion. We have shown how low radiative efficiency accretion models can possibly provide the underlying scalings that most easily explain the properties of the observed fundamental plane. Radiatively efficient thin disc-corona systems are clearly inconsistent with the data. The only possibility for these models to be reconciled with our observations would entail a highly radiatively inefficient corona, where most of the dissipated magnetic energy is converted into bulk kinetic energy of outflowing gas, as described by Merloni & Fabian (2002). This would require some specific model for the magnetic dissipation processes, and for their scaling with  $M$  and  $\dot{m}$ , which are currently unknown.

However, because both such modes of accretion are expected to occur only below accretion rates  $\lesssim$  few percent of Eddington, we would expect the  $\log M - \log L_R - \log L_X$  correlation to break down at around this limit. In other words, we expect the QSOs and the bright Seyferts in our sample, which occupy the region of high accretion rates and are independently known to have spectral characteristics inconsistent with models of low radiative efficiency, to display significantly more scatter. In order to illustrate this point further, in Figure 8 we plot, as a function of the ratio  $L_X/L_{\text{Edd}}$ , the radio luminosity divided by  $M^{1.38}$  (such a scaling for the radio luminosity with mass is obtained directly from the fundamental plane equation (13) by imposing that the X-ray luminosity scales linearly with black hole mass). As indeed expected, by rescaling the radio luminosity in such a way all the different tracks corresponding to different mass bins in Fig. 3b collapse into a single one (with some residual scatter). The region between the two vertical lines corresponds to the expected values of  $L_X/L_{\text{Edd}}$  above which a change of accretion mode, from radiatively inefficient to standard radiatively efficient is expected to occur.

In GBHs, it had indeed been shown that the correlation between radio and X-ray luminosity breaks down as the sources switch to their high states (Maccarone 2003; Gallo, Fender, & Pooley 2003). In particular, high luminosity states of GBH (high or very high states) show highly variable radio fluxes and radio to X-ray ratios (Mirabel & Rodriguez 1994; Fender et al. 1999). If this reflects a general property of the disc-jet coupling at high accretion rates, a substantial increase in the scatter should appear above the critical accretion rate. Our SMBH sample is still limited in order to test whether a similar behavior is observed. In fact, we select out of our sample the majority of bright quasars, both radio quiet and radio loud, because of the lack of a reliable mass estimates for these sources. However, there is some hint of a possible gap in the distribution of  $L_X/L_{\text{Edd}}$  (bottom right panel of Figure 1) in the region around the critical accretion rate, and perhaps also an apparent increase in the scatter about the correlation between radio and X-ray luminosity (conveniently rescaled with the BH masses), as seen in Figure 8.

We may thus speculate that the famous (and still much debated, see e.g. Cirasuolo et al. 2003) radio loud/radio quiet dichotomy of quasars will appear only at the highest values of  $\dot{m}$ , and be caused mainly by a switch of accretion mode analogous to

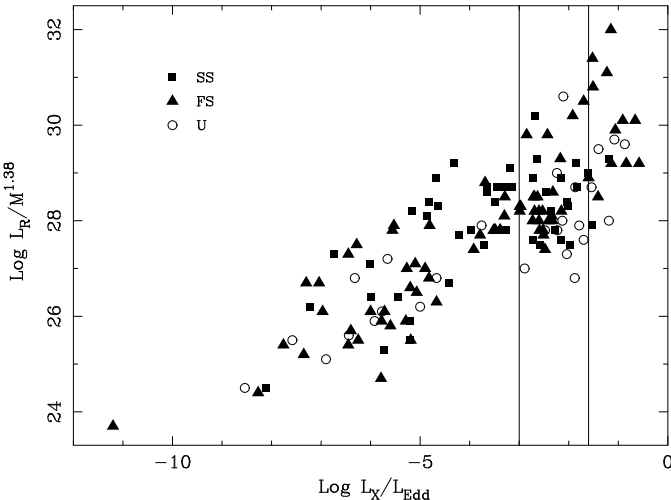


**Figure 8.** The radio luminosity  $\log L_R$ , divided by  $M^{1.38}$  as a function of the ratio  $L_X/L_{\text{Edd}}$ . Solid squares are for steep spectrum sources, solid triangles for flat spectrum ones and open circles for sources with undetermined radio spectral index. Two vertical lines mark the boundary of the region where we expect the critical luminosity for the mode change between radiatively inefficient and efficient accretion. The scaling for the radio luminosity with mass is obtained directly from the fundamental plane equation (13) by imposing that the X-ray luminosity scales linearly with black hole mass.

the high/very high transition in GBH. At low accretion rates, black holes seem to follow the more regular behavior circumscribed by the fundamental plane of eq. (13). A note of caution is obviously in order here because of the limited statistics upon which our sample is based.

## 7 SUMMARY

We have shown how the coupling between accretion flows and jet emission in black holes can be understood by studying large samples of *both* galactic (GBH) and supermassive (SMBH) black holes with measured mass, observed at both radio and X-ray wavelengths.

We have compiled, from the existing literature, a sample of  $\sim 100$  supermassive black holes and  $\sim 50$  different observations of galactic, stellar mass black holes. We required that the SMBH have a reliable measure of the central black hole mass, either (preferentially) direct, via high resolution kinematics studies of surrounding stars and gas or reverberation mapping of the broad line region (for luminous Seyfert 1 galaxies and Quasars), or, indirectly, thanks to the empirical correlation between black hole masses and central velocity dispersion. Although such selection criteria introduce a number of biases in the final distribution of  $M$ , which are difficult to control, our final sample spans a large enough range in both mass and accretion rate to unveil major trends in the physical properties of active black holes. This is a crucial point, and represents the main novelty of our approach. Most previous studies on the subject have only considered correlations of jet (radio) luminosity with black hole mass or with luminosity in other wavewbands (and hence with accretion rate) separately.

We have performed a partial correlation analysis on the sample, and concluded that the radio luminosity is strongly correlated with *both* black hole mass *and* X-ray luminosity, while in turn, the X-ray luminosity correlates with both mass and radio luminosity.

In light of this, we have carried out a multivariate linear regression analysis and derived the best fit correlation coefficient between radio luminosity, X-ray luminosity and black hole mass.

The data from the entire sample allow us to put tight constraints on the correlation coefficients. Remarkably, we find that the sources lie preferentially on a plane (“the fundamental plane of black hole activity”) in the three dimensional ( $\log L_R, \log L_X, \log M$ ) space, described by the equation  $\log L_R = (0.60^{+0.11}) \log L_X + (0.78^{+0.11}) \log M + 7.33^{+4.05}_{-4.07}$ . The scatter around this plane is, however, significant ( $\sigma_R = 0.88$ ).

From a theoretical point of view, these results clearly suggest that the *ansatz* of scale invariance for the disc-jet coupling (Heinz & Sunyaev 2003) captures the main physical properties of such systems. Thus, a universal theoretical scaling between the radio flux at a given frequency and both mass and accretion rate can be derived, *independently of the jet model*, with scaling indices that depend only on the (observable) spectral slope of the synchrotron emission in the radio band, and on the accretion mode. Also, it is possible to predict the correct amount of scatter for any such relationship.

By comparing the observationally derived correlation coefficients to the theoretically predicted ones, we are able to put constraints on accretion models and on the disc-jet coupling. We demonstrate that the X-ray emission from black holes accreting at less than a few per cent of the Eddington rate cannot be produced by radiatively efficient accretion, while radiatively inefficient accretion flows agree well with the data. The optically thin X-ray jet synchrotron emission model is only marginally consistent with the observed correlation; however, cooling of the electrons should be properly taken into account before drawing a firmer conclusion on the issue.

More accurately selected samples of more luminous sources, including a significant number of both radio quiet and loud quasars with well determined radio spectral properties, should allow the observation of bends, discontinuities or even bifurcations of the fundamental plane associated with accretion mode switches and with the turning on and off of the most powerful radio sources.

## ACKNOWLEDGMENTS

We are grateful to Marat Gilfanov for his useful comments. We thank Eric Feigelson and the Statistical Consulting Center for Astronomy (SDASS) for providing the code for the partial correlation analysis and some advice on its usage. This research has made use of the NASA/IPAC extragalactic database (NED), which is operated by the Jet Propulsion Laboratory, Caltech, under contract with NASA. We have also made use of LEDA, supplied by the LEDA team at the CRAL-Observatoire de Lyon. This research has made use of the publicly available radio monitoring data from the Green Bank Interferometer. The Green Bank Interferometer is a facility of the National Science Foundation operated by the NRAO in support of NASA High Energy Astrophysics programs. This research made use of results provided by the ASM/RXTE teams at MIT and at the RXTE SOF and GOF at NASA’s GSFC.

## REFERENCES

- Abramowicz M. A., Chen X., Kato S., Lasota J.-P., & Regev O., 1995, *ApJL*, 438, L37.  
 M.A. Abramowicz, 1998, in *Theory of Black hole accretion disks*, eds. M.A. Abramowicz, G. Bjornsson, and J.E. Pringle. (CUP, 1998)

- Akritas, M. G. & Siebert, J., 1996, MNRAS, 278, 919
- Allen S. W., Fabian A. C., Johnstone R. M., Arnaud K. A. & Nulsen P. E. J., 2001, MNRAS, 322, 589
- Baganoff et al., 2001, Nature, 413, 45.
- Balbus S. A. & Hawley J. F., 2002, ApJ, 573, 749
- Barth, A. J., Ho, L. C., & Sargent, W. L. W., 2002, AJ, 124, 2607
- Bassani, L., Dadina, M., Maiolino, R., Salvati, M., Risaliti, G., della Ceca, R., Matt, G., & Zamorani, G., 1999, ApJS, 121, 473
- Becker, R. H., White, R. L., & Edwards, A. L., 1991, ApJS, 75, 1
- Begelman M. C., Blandford R. D., & Rees M. J., 1984, Rev. Mod. Phys., 56, 255
- Blandford R. D. & Königl A., 1979, ApJ, 232, 34
- Brinkmann W., Laurent-Muehleisen S. A., Voges W., Siebert J., Becker R. H., Brotherton M. S., White R. L., & Gregg M. D., 2000, A&A, 356, 445
- Churazov E., Forman W., Jones C. & Böhringer H., 2003, ApJ, in press. astro-ph/0301482
- Corbel, S., Nowak, M. A., Fender, R. P., Tzioumis, A. K., & Markoff, S., 2003, A&A, in press. astro-ph/0301436
- De Rosa, A., Fabian, A. C., & Piro, L., 2002, MNRAS, 334, L21
- De Zeeuw T., 2003, to appear in Carnegie Observatories Astrophysics Series, Vol. 1: "Coevolution of black holes and galaxies" ed. L.C. Ho (Cambridge: CUP)
- Dhawan, V., Pooley, G. G., Ogle, R. N., & Mirabel, I. F., 2000, IAUC 7395
- Di Matteo, T., Allen, S. W., Fabian, A. C., Wilson, A. S., & Young, A. J., 2003, ApJ, 582, 133
- Di Matteo, T., Celotti, A., & Fabian, A. C., 1999, MNRAS, 304, 809
- Di Matteo, T., Johnston, R. M., Allen, S. W., & Fabian, A. C., 2001, ApJL, 550, L19
- Di Matteo T., Quataert E., Allen S. W., Narayan R., & Fabian A. C., 2000, MNRAS, 311, 507
- Dolan J. F., 1992, ApJ, 384, 249.
- Done, C., 2002, Phil. Trans. of the Royal Society, A360, 1967.
- Esin, A. A., McClintock, J. E., & Narayan, R., 1997, ApJ, 489, 865.
- Fabbiano, G., Kim, D.-W., & Trinchieri, G., 1992, ApJS, 80, 531
- Fabbiano, G., et al., 2003, ApJ, in press. astro-ph/0301297
- Falcke, H. & Biermann, P. L., 1995, A&A, 293, 665
- Falcke, H. & Biermann, P. L., 1996, A&A, 308, 321
- Falcke, H., Malkan, M. A., & Biermann, P. L., 1995, A&A, 298, 375
- Falcke, H., Nagar, N. M., Wilson, A. S., & Ulvestad, J. S., 2000, ApJ, 542, 197
- Fasano G. & Vio R., 1988, Newsletter of the Working Group for Modern Astronomical Methodology, 7, 2
- Fender R. P., Garrington S. T., McKay D. J., Muxlow T. W. B., Pooley G. G., Spencer R. E., Stirling A. M., & Waltman E. B., 1999, MNRAS, 304, 865
- Fender, R. P., Hjellming, R. M., Tilanus, R. P. J., Pooley, G. G., Deane, J. R., Ogle, R. N., & Spencer, R. E., 2001, MNRAS, 322, L23
- Fender, R. P. & Kuulkers, E., 2001, MNRAS, 324, 923
- Ferrarese L., 2002, in "Current High Energy Emission around Black Holes", ed. C.-H. Lee (Singapore: World Scientific) in press. astro-ph/0203047
- Ferrarese, L. & Merritt, D., 2000, ApJL, 539, L9
- Filippenko A. V. & Chornock R., 2001, IAUC 7644
- Franceschini, A., Vercellone, S., & Fabian, A. C., 1998, MNRAS, 297, 817
- Frank, J., King, A., & Raine, D., 2002, *Accretion power in astrophysics*, 3rd ed. (CUP, 2002)
- Frontera et al., 2001, ApJ, 561, 1006
- Gallo, E., Fender, R. P., & Pooley, G. G., 2002, in 'Proceedings of the 4th Microquasar Workshop', Eds. P.Durochoux, Y.Fuchs and J.Rodriguez. Center for Space Physics: Kolkata (India), p.201.
- Gallo, E., Fender, R. P., & Pooley, G. G., 2003, MNRAS, in press. astro-ph/0305231
- Gebhardt, K. et al. ApJL, 539, L13
- George, I. M., Turner, T. J., Yaqoob, T., Netzer, H., Laor, A., Mushotzky, R. F., Nandra, K., & Takahashi, T., 2000, ApJ, 531, 52
- Giovannini, G., Cotton, W. D., Feretti, L., Lara, L., & Venturi, T., 1998, ApJ, 493, 632
- Gondoin, P., Orr, A., Lumb, D., & Santos-Leo, M., 2002, A&A, 388, 74
- Gregory, P. C. & Condon, J. J., 1991, ApJS, 75, 1011
- Greiner, J., Cuby, J. G., & McCaughrean, M. J., 2001, Nature, 414, 522
- Griffith, et al., 1995, ApJS, 97, 347
- Grimm, H.-J., Gilfanov, M., & Sunyaev, R., 2002, A&A, 391, 923
- Haardt, F. & Maraschi, L., 1991, ApJL, 380, L51
- Hanson M. M., Still M. D., & Fender R. P., ApJ, 541, 308
- Hawley J. F. & Balbus S. A., 2002, ApJ, 573, 749
- Heinz, S., 2002, A&A, 388, 40
- Heinz, S. & Sunyaev, R. A., MNRAS, submitted. astro-ph/0305252
- Héraudeau, Ph. & Simien, F., 1998, A&ASS, 113, 317
- Ho, L. C., 2002a, ApJ, 564, 120
- Ho, L. C., Filippenko, A. V., & Sargent, W. L., 1997b, ApJ, 487, 568
- Ho, L. C., Filippenko, A. V., & Sargent, W. L., 1997a, ApJS, 112, 315
- Ho, L. C. & Peng, C. Y., 2001, ApJ, 555, 650
- Ho, L. C., Terashima, Y., & Ulvestad, J. S., 2003, ApJ, in press. astro-ph/0303060
- Ho, L. C. & Ulvestad, J. S., 2001, ApJS, 133, 77
- Ho, L. C., et al., 2001, ApJL, 549, L51
- Igumenschev I. V. & Abramowicz M. A., 2000, ApJS, 130, 463
- Isobe, T., Feigelson, E. D., & Nelson, P. I., 1986, ApJ, 306, 490
- Kaaret P., Corbel S., Prestwich A. H., & Zezas A., 2003, Science, 299, 365
- Kaspi, S., Smith, P. S., Netzer, H., Maoz, D., Jannuzi, B. T., & Giveon, U., 2000, ApJ, 533, 631
- Kellermann K. I., Sramek R., Schmidt M., Shaffer D. B., & Green R., 1989, AJ, 98, 1195
- Kojoian, G., Tovmasian, Kh. M., Dickinson, D. F., & Dinger, A. S. C., 1980, AJ, 85, 1462
- Kormendy, J. & Richstone, D., ARA&A, 33, 581
- Lacy, M., Laurent-Muehleisen, S. A., Ridgway, S. E., Becker, R. H., & White, R., 2001, ApJL, 551, L17
- Laor, A., 2000, ApJL, 543, L111
- Lawson, A. J., & Turner, M. J. L., MNRAS, 288, 920
- Leighly, K. M., 1999, ApJS, 125, 317
- Loewenstein, M., Mushotzky, R. F., Angelini, L., Arnaud, K. A., & Quataert, E., 2001, ApJL, 555, L21
- Maccarone T., 2003, MNRAS, submitted.
- Magorrian, J. et al., 1998, AJ, 115, 2285
- Makishima K. et al., 2000, ApJ, 535, 632
- Markoff S., Falcke H., & Fender R., 2001, A&A, 372, L25
- Markoff, S., Nowak, M., Corbel, S., Fender, R., & Falcke, H., 2003, A&A, 397, 645
- McLure, R. J. & Dunlop, J. S., 2001, MNRAS, 327, 199
- Melia, F. & Falcke, H., 2001, Ann. Rev. Astron. Astrophys., 39, 309
- Merloni, A., 2003, MNRAS in press. astr-ph/0302074
- Merloni, A. & Fabian, A. C., 2002, MNRAS, 332, 165
- Merritt, D. & Ferrarese, L., 2001, MNRAS, 320, L30
- Miley G. K., 1980, ARA&A, 18, 165
- Mirabel, I. F. & Rodriguez, L. F., 1994, Nature, 371, 46
- Moran, E. C., Kay, L. E., Davis, M., Filippenko, A. V., & Barth, A. J., 2001, ApJ, 556, 75
- Nagar, N. M., Falcke, H., Wilson, A. S., & Ulvestad, J. S., 2002, A&A, 392, 53
- Nandra, K., George, I. M., Mushotzky, R. F., Turner, T. J., & Yaqoob, T., 1997, ApJ, 477, 602
- R. Narayan, 2002, In Proceedings of *Lighthouses of the Universe* eds. M. Gilfanov, R. Sunyaev et al., (Springer-Verlag, 2002).
- Narayan R., Barrett D., & McClintock J. E., 1997,
- Narayan R., Garcia M. R., & McClintock J. E., 1997, ApJL, 478, L79
- Narayan R., Igumenschev I. V., & Abramowicz M. A., 2000, ApJ, 539, 798
- Narayan R., Mahadevan R., Grindley J. E., Popham R. G., & Gammie C., 1998a, 492, 554
- Narayan, R., Mahadevan, R., & Quataert, E., 1998b, in *Theory of Black hole accretion disks*, eds. M.A. Abramowicz, G. Bjornsson, and J.E. Pringle. (CUP, 1998)
- Narayan R., Quataert, E., Igumenschev I. V., & Abramowicz M. A., 2002, ApJ, 577, 295
- Narayan, R. & Yi, I., 1994, ApJL, 428, L13
- Narayan R. & Yi I., 1995, ApJL, 452, 710

- Oshlack A. Y. K. N., Webster R. L., & Whiting M. T., 2002, *ApJ*, 576, 81
- Orosz, J. A. & Bailyn, C. D., 1997, *ApJ*, 477, 876
- Pellegrini, S., Venturi, T., Comastri, A., Fabbiano, G., Fiore, F., Vignali, C., Moraganti, R., & Trincheri, G., 2003, *ApJ*, in press. astro-ph/0211322
- Polletta, M., Bassani, L., Malaguti, G., Palumbo, G. G. C. & Caroli, E., 1996, *ApJS*, 106, 399
- Pounds, K., Reeves, J., O'Brien, P., Page, K., Turner, M., & Nayakshin, S., 2001, *ApJ*, 559, 181
- Press, W. H., Teukolsky, S. A., Vetterling, W. T., & Flannery, B. P., 1992, *Numerical Recipes* (2nd ed.; Cambridge: CUP)
- Quataert E., Di Matteo T., Narayan R. & Ho L. C., 1999, *ApJL*, 525, L89
- Rawlings S. & Saunders R., 1991, *Nature*, 349, 138
- Rees M. J., Phinney E. S., Begelman M. C., & Blandford R. D., 1982, *Nature*, 295, 17
- Rush, B., Malkan, M. A., & Edelson, R. A., 1996, *ApJ*, 473, 130
- Rybicki G. B. & Lightman A. P., 1979, *Radiative processes in astrophysics* (New York: Wiley)
- Saglia, et al., 1993, *ApJ*, 403, 567
- Sambruna, R. M., Eracleous, M., & Mushotzky, R. F., 1999, *ApJ*, 526, 60
- Sams B. J., Eckart A., & Sunyaev R., 1996, *Nature*, 382, 47
- Schödel, R. et al., 2002, *Nature*, 419, 694
- Shakura, N. I. & Sunyaev, R. A., 1973, *A&A*, 24, 337
- Shih, D. C., Iwasawa, K., & Fabian, A. C., 2003, *MNRAS* in press. astro-ph/0302108
- Simien, F. & Prugniel, Ph., 2002, *A&A*, 384, 371, and the HYPERLEDA catalogue: <http://www-obs.univ-lyon1.fr/hypercat/>
- Stirling, A. M., Spencer, R. E., de la Force, C. J., Garrett, M. A., Fender, R. P., & Ogle, R. N., 2001, *MNRAS*, 327, 1273
- Tadhunter, C., Marconi, A., Axon, D., Wills, K., Robinson, T. G., & Jackson, N., 2003, *MNRAS*, in press. astro-ph/0302513
- Terashima, Y., Iyomoto, N., Ho, L. C., & Ptak, A. F., 2002, *ApJS*, 139, 1
- Terashima, Y. & Wilson, A. S., 2003, *ApJ*, 583, 145
- Thean, A., Pedlar, A., Kukula, M. J., Baum, S. A., & O'Dea, C. P., 2001, *MNRAS*, 325, 737
- Tremaine, S., et al., 2002, *ApJ*, 574, 554
- Turner, T. J. & Pounds, K. A., 1989, *MNRAS*, 240, 833
- Ulvestad, J. S., Antonucci, R. R., & Goodrich, R. W., 1995, *AJ*, 109, 81
- Ulvestad, J. S. & Wilson, A. S., 1989, *ApJ*, 343, 659
- Verlome, E. K. et al., 2002, *MNRAS*, 335, 517
- Véron-Cetty, M. P. & Véron, P., 2001, *A&A*, 374, 92
- Wagner, R. M., Foltz, C. B., Shahbaz, T., Charles, P. A., Starrfield, S. G., & Hewett, P., 2001, *ApJ*, 556, 42
- Wang, T. & Lu, Y., 2001, *A&A*, 377, 52
- Weaver, K. A., Gelbord, J., & Yaqoob, T., 2001, *ApJ*, 550, 261
- White, N. E., Giommi, P., & Angelini, L., 2000, WGACAT. VizieR On-line Data Catalog: IX/31
- Willott C. J., Rawlings S., Blundell K. M. & Lacy M., 1999, *MNRAS*, 309, 1017
- Woo, J. & Urry, C. M., 2002, *ApJ*, 579, 530
- Young, A. J., Wilson, A. C., Arnaud, K. A., Terashima, Y., & Smith, D. A., 2002, *ApJ*, 564, 176
- Zdziarski A. A., Gilfanov M., Lubinski P., & Revnivtsev M., 2003, *MNRAS*, in press. astro-ph/0209363
- Zhou, H. & Wang, T., 2002, *Chin. J. Astron. Astrophys.*, 2, 501.